Title page

Title:

Stretch Regulates Alveologenesis Via Mesenchymal $G_{\alpha q/11}$-Mediated TGFβ2 Activation

Authors:

Amanda T Goodwin[1*]

Alison E John[1]

Chitra Joseph[1]

Anthony Habgood[1]

Amanda L Tatler[1]

Stefan Offermanns[2]

Neil C Henderson[3,4]

Gisli Jenkins[1]

1) Nottingham NIHR Respiratory Biomedical Research Centre, University of Nottingham, UK
2) Max Planck Institute for Heart and Lung Research, Bad Nauheim, Germany
3) Centre for Inflammation Research, University of Edinburgh, UK
4) MRC Human Genetics Unit, Institute of Genetics and Molecular Medicine, University of Edinburgh, Edinburgh, UK.

***Correspondence to:** Amanda T Goodwin – Amanda.goodwin@nottingham.ac.uk

Summary

Alveolar development requires tight spatiotemporal regulation of numerous signalling pathways that are influenced by chemical and mechanical stimuli. Pericytes, perivascular mesenchymal cells, are key lung progenitor cells that are important for many developmental processes. Transforming growth factor-β (TGFβ) is essential for alveologenesis, and the G protein α subunits $G_{\alpha q}$ and $G_{\alpha 11}$ ($G_{\alpha q/11}$) can transmit mechanical and chemical signals to activate TGFβ in epithelial cells. To understand the role of mesenchymal $G_{\alpha q/11}$ in lung TGFβ signalling and lung development, we generated a mesenchymal $G_{\alpha q}$ /$G_{\alpha 11}$ knockout mouse (*Pdgfrb-Cre*$^{+/-}$;*Gnaq*$^{fl/fl}$;*Gna11*$^{-/-}$). *Pdgfrb-Cre*$^{+/-}$;*Gnaq*$^{fl/fl}$;*Gna11*$^{-/-}$ mice exhibited abnormal alveolar development, with evidence of suppressed pericyte to myofibroblast differentiation and reduced lung TGFβ2 deposition. Cyclical mechanical stretch-induced TGFβ activation required $G_{\alpha q/11}$ signalling and serine protease activity, but was independent of integrins, suggesting a role for TGFβ2. These data highlight a previously undescribed mechanism of cyclical stretch-induced $G_{\alpha q/11}$-dependent TGFβ2 signalling in mesenchymal cells, which is imperative for normal alveologenesis.

Key words: Alveolarisation, alveologenesis, TGFβ, $G_{\alpha q/11}$, GPCR, lung development, cyclical mechanical stretch

Introduction

Normal alveologenesis requires the tight spatiotemporal control of numerous molecular signalling pathways, and coordinated crosstalk between multiple cell types. Any perturbation to these complex processes can disturb the formation of the alveoli, resulting in structural and functional abnormalities to the gas exchange regions of the lungs. Such abnormalities contribute to perinatal death and lifelong lung function disturbances in survivors. The alveolar stage is the final phase of lung development, during which primitive pulmonary sacculi are divided by newly formed secondary septae to form mature alveoli. Alveolarisation occurs between 36 weeks gestation to around 6 years of age in humans (Donahoe et al., 2016), and postnatal days 3-30 (P3-P30) in mice (Beauchemin et al., 2016; Li et al., 2015; Pozarska et al., 2017), therefore postnatal exposures and stimuli are key influences in alveolar development.

Pericytes are widely considered to be mesenchymal precursor cells in the lung, and are integral to multiple developmental processes (Barron et al., 2016; Kato et al., 2018; Ricard et al., 2014). Pericytes are perivascular in location, but also migrate and differentiate into parenchymal myofibroblasts. Myofibroblast-driven deposition of extracellular matrix (ECM) proteins, such as collagen and elastin, provide the essential scaffolds for secondary septation (Mecham, 2018; Mizikova and Morty, 2015). Therefore pericytes, and the mesenchymal cells that derive from them, are instrumental in alveologenesis.

The pleiotropic cytokine transforming growth factor-β (TGFβ) regulates numerous developmental processes, including the proliferation, migration, and differentiation of pericytes (Bartram and Speer, 2004), and the generation of ECM. TGFβ signalling is tightly regulated in vivo by the production of TGFβ in latent form, and the three mammalian TGFβ isoforms must be activated in order to exert their biological effects. While TGFβ signalling is essential for multiple processes in alveolar development (Bartram and Speer, 2004), the mechanisms that control TGFβ activation in alveologenesis are unclear.

Latent TGFβ is activated when a conformational change to the large latent complex alters the relationship between TGFβ and the latency associated peptide, allowing TGFβ to interact with its receptor. The G-proteins $G_{\alpha q}$ and $G_{\alpha 11}$ ($G_{\alpha q/11}$) mediate TGFβ activation in response to G-protein-coupled receptor (GPCR)-ligand binding as well as mechanical stretch in epithelial cells (John et al., 2016; Xu et al., 2009). GPCR signalling has also been implicated in normal alveologenesis (Funke et al., 2016). Cyclical mechanical stretch (CMS) has been shown to induce TGFβ activation in lung slices via a Rho-associated kinase (ROCK)- and αv integrin-dependent process (Froese et al., 2016), although the contribution to this by individual cell types is unknown. While stretch secondary to foetal breathing

movements in utero is essential for early lung development (Donahoe et al., 2016), the role of breathing-related CMS specifically in mesenchymal cells in alveolar development has not been investigated.

We hypothesised that $G_{\alpha q/11}$ would mediate CMS-induced TGFβ activation via ROCK and integrin signalling in mesenchymal cells, and that this would be important in alveologenesis. Here we show, using a mesenchymal $G_{\alpha q/11}$ knockout mouse model and an in vitro CMS system, that mesenchymal $G_{\alpha q/11}$ is essential for normal alveologenesis via CMS-induced TGFβ signalling, but in a ROCK and integrin-independent manner.

Results

Pdgfrb-Cre$^{+/-}$*;Gnaq*$^{fl/fl}$*;Gna11*$^{-/-}$ mice are growth restricted and are not viable beyond P24

To understand whether mesenchymal $G_{\alpha q/11}$ deletion resulted in detrimental effects in vivo, the genotype frequencies from the *Pdgfrb-Cre*$^{+/-}$ *x Gnaq*$^{fl/fl}$*;Gna11*$^{-/-}$ crosses were analysed. Fewer mesenchymal $G_{\alpha q/11}$ knockout (*Pdgfrb-Cre*$^{+/-}$*;Gnaq*$^{fl/fl}$*;Gna11*$^{-/-}$) pups reached genotyping age (2 weeks old, P14) than was expected (6.6% observed compared with 12.5% expected, Chi squared value = 22.03, $p<0.005$, **Figure 1A**). Conversely, mice that possessed at least one functional mesenchymal *Gnaq* or *Gna11* allele reached genotyping age at rates closer to the expected Mendelian frequencies (**Figure 1A**). Furthermore, *Pdgfrb-Cre*$^{+/-}$*;Gnaq*$^{fl/fl}$*;Gna11*$^{-/-}$ pups were notably smaller than littermates with at least one intact mesenchymal *Gnaq* or *Gna11* allele. *Pdgfrb-Cre*$^{+/-}$*;Gnaq*$^{fl/fl}$*;Gna11*$^{-/-}$ animals had a mean weight 1.9-3.2g lower than all other genotypes (5.4g vs 7.3-8.4g, $p<0.03$ **Figure 1B**). *Pdgfrb-Cre*$^{+/-}$*;Gnaq*$^{fl/fl}$*;Gna11*$^{-/-}$ pups were also smaller in physical size compared with control animals (**Figure 1C**). There was no sex-related difference in weight across genotypes (**Figure 1D**). These findings indicate that mesenchymal $G_{\alpha q/11}$ deletion causes a detrimental developmental phenotype, leading to death in utero or in early life.

The first two *Pdgfrb-Cre*$^{+/-}$*;Gnaq*$^{fl/fl}$*;Gna11*$^{-/-}$ mice from this breeding programme were humanely killed due to very poor physical condition at P21 and P24. Therefore, all further analyses were performed at P14. *Gnaq*$^{fl/fl}$*;Gna11*$^{-/-}$ mice develop normally and do not express a phenotype (John et al., 2016), therefore mice with this genotype were used as controls for all further analyses (referred to as *Gna11*$^{-/-}$ controls).

Pdgfrb-Cre$^{+/-}$*;Gnaq*$^{fl/fl}$*;Gna11*$^{-/-}$ mice have impaired alveologenesis.

To understand the role of mesenchymal $G_{\alpha q/11}$ signalling in lung development, the lungs of *Pdgfrb-Cre*$^{+/-}$*;Gnaq*$^{fl/fl}$*;Gna11*$^{-/-}$ mice and *Gna11*$^{-/-}$ controls were examined histologically.

Pdgfrb-Cre$^{+/-}$*;Gnaq*$^{fl/fl}$*;Gna11*$^{-/-}$ mouse lungs exhibited clear abnormalities consistent with impaired alveolar development at P14 (**Figure 2A**). *Pdgfrb-Cre*$^{+/-}$*;Gnaq*$^{fl/fl}$*;Gna11*$^{-/-}$ lungs contained enlarged airspaces with a mean linear intercept distance of 63.47µm compared with 36.43µm in *Gna11*$^{-/-}$ mice (p=0.03, **Figure 2B**), thickened alveolar walls of 12.2µm compared with 7.0µm in *Gna11*$^{-/-}$ controls (p=0.03, **Figure 2C**), and fewer secondary crests (53.7 vs 107.2 per field, p=0.03, **Figure 2D**) relative to *Gna11*$^{-/-}$ littermate controls.

In addition to these structural abnormalities, *Pdgfrb-Cre*$^{+/-}$*;Gnaq*$^{fl/fl}$*;Gna11*$^{-/-}$ lungs expressed lower levels of the proliferative marker Ki67 than *Gna11*$^{-/-}$ controls, with 16% of cell nuclei staining positively for Ki67 in *Pdgfrb-Cre*$^{+/-}$*;Gnaq*$^{fl/fl}$*;Gna11*$^{-/-}$ lungs compared with 26% in *Gna11*$^{-/-}$ controls (p=0.03, **Figure 2A, 2E**). Furthermore, *Pdgfrb-Cre*$^{+/-}$*;Gnaq*$^{fl/fl}$*;Gna11*$^{-/-}$ lungs contained a lower proportion of cells staining positively for the type II epithelial cell marker pro-surfactant protein C (pro-SPC) than *Gna11*$^{-/-}$ controls lungs, at 8.9% and 12.8% of all cells, respectively (**Figure 2A, 2F**).

Finally, *Pdgfrb-Cre*$^{+/-}$*;Gnaq*$^{fl/fl}$*;Gna11*$^{-/-}$ lungs were heavier relative to total body weight compared with lungs from *Gna11*$^{-/-}$ mice (16.5 vs 14.3mg/g total body weight, p<0.01, **Figure 2G**), suggesting elevated lung density in these animals. Overall, these structural, proliferative, and cellular differentiation abnormalities indicate a disturbance to alveologenesis in *Pdgfrb-Cre*$^{+/-}$*;Gnaq*$^{fl/fl}$*;Gna11*$^{-/-}$ mice.

Myofibroblast differentiation and function is defective in *Pdgfrb-Cre*$^{+/-}$*;Gnaq*$^{fl/fl}$*;Gna11*$^{-/-}$ mouse lungs

As myofibroblasts play essential roles in normal alveolar development, studies were undertaken to assess myofibroblast differentiation and function in *Pdgfrb-Cre*$^{+/-}$*;Gnaq*$^{fl/fl}$*;Gna11*$^{-/-}$ lungs.

Immunohistochemical staining for the myofibroblast marker α-smooth muscle actin (αSMA) demonstrated fewer myofibroblasts in the lungs of P14 *Pdgfrb-Cre*$^{+/-}$*;Gnaq*$^{fl/fl}$*;Gna11*$^{-/-}$ mice compared with *Gna11*$^{-/-}$ littermate controls (**Figure 3A**). While overall αSMA staining was decreased in *Pdgfrb-Cre*$^{+/-}$*;Gnaq*$^{fl/fl}$*;Gna11*$^{-/-}$ lungs, there was no significant reduction in the proportion of αSMA-positive secondary crests compared with *Gna11*$^{-/-}$ lungs (0.69 vs 0.84 in controls, p =0.2, **Figure 3B**).

To investigate whether $G_{\alpha q/11}$ knockout influences myofibroblast differentiation, murine embryonic fibroblasts (MEFs) that were wild-type (WT), $G_{\alpha q/11}$ deficient (*Gnaq*$^{-/-}$*;Gna11*$^{-/-}$) or $G_{\alpha 12/13}$ deficient (*Gna12*$^{-/-}$*;Gna13*$^{-/-}$) were assessed for αSMA protein and Acta2 mRNA expression. MEFs with a long-term deficiency in $G_{\alpha q/11}$ had lower Acta2 mRNA (**Figure 3C**) and αSMA protein expression (**Figure 3D, 3E**) than WT MEFs, whereas MEFs lacking $G_{\alpha 12/13}$, another G_{α} subunit family, did not have significantly different αSMA expression

compared with WT cells. This implies a key role for $G_{\alpha q/11}$ signalling in the differentiation of myofibroblasts from mesenchymal precursor cells.

Pdgfrb-Cre$^{+/-}$*;Gnaq*$^{fl/fl}$*;Gna11*$^{-/-}$ lungs also showed evidence of defective myofibroblast synthetic function. *Pdgfrb-Cre*$^{+/-}$*;Gnaq*$^{fl/fl}$*;Gna11*$^{-/-}$ lungs contained fewer elastin fibres (7.4 vs 24.9 fibres per field, p=0.03, **Figure 3A, 3F**) and fewer elastin-positive secondary crests (57.5% vs 84.8%, p=0.03, **Figure 3G**) than *Gna11*$^{-/-}$ mouse lung. Furthermore, picrosirius red staining revealed that P14 *Pdgfrb-Cre*$^{+/-}$*;Gnaq*$^{fl/fl}$*;Gna11*$^{-/-}$ mouse lungs contained less collagen than the lungs of *Gna11*$^{-/-}$ controls (**Figure 3A, row 3-5**). These data were supported by lower *Eln*, *Col1a1* and *Col3a1* mRNA expression in *Gnaq*$^{-/-}$*;Gna11*$^{-/-}$ MEFs than WT MEFs (**Figure 3H-J**). These data imply a failure of myofibroblast differentiation in the lungs of mice lacking mesenchymal $G_{\alpha q/11}$ associated with a reduction in myofibroblast function, leading to a reduction in subepithelial matrix deposition.

Pdgfrb-Cre$^{+/-}$*;Gnaq*$^{fl/fl}$*;Gna11*$^{-/-}$ mice have abnormal peripheral pulmonary vessels

Pericytes are important precursor cells to pulmonary myofibroblasts, and originate from the perivascular region. Therefore, we examined the pulmonary vasculature histologically to assess for abnormalities caused by mesenchymal $G_{\alpha q/11}$ deletion. P14 *Pdgfrb-Cre*$^{+/-}$*;Gnaq*$^{fl/fl}$*;Gna11*$^{-/-}$ lungs contained markedly abnormal peripheral pulmonary vessels (**Figure 4A-F**), with significantly thicker walls than the peripheral pulmonary vessels of *Gna11*$^{-/-}$ controls (mean maximum wall thickness 16.4 vs 7.3µm, p=0.03, **Figure 4G**). These vessel walls did not contain significant elastin or collagen layers (**Figure 4B-C)**, and consisted of a thin CD31 positive endothelial layer (**Figure 4D**) surrounded by a thickened αSMA positive vascular smooth muscle layer (**Figure 4E**), without a high proliferative rate (Ki67 positive; **Figure 4F**), indicating that the smooth muscle layer was hypertrophic rather than hyperplastic. Given the similarity in appearance of the abnormal peripheral pulmonary vasculature in *Pdgfrb-Cre*$^{+/-}$*;Gnaq*$^{fl/fl}$*;Gna11*$^{-/-}$ lungs to those seen in pulmonary arterial hypertension, we assessed the hearts from these animals for evidence of right ventricular hypertrophy. We found no difference in right: left ventricular wall ratio in *Pdgfrb-Cre*$^{+/-}$*;Gnaq*$^{fl/fl}$*;Gna11*$^{-/-}$ mice relative to controls (**Figure S1**). These data suggest a primary pericyte migration and differentiation defect, rather than secondary pulmonary hypertension due to impaired alveologenesis.

Cyclical mechanical stretch-induced TGFβ activation in fibroblasts requires $G_{\alpha q/11}$, but not ROCK or αv or β1 integrins

Given the crucial roles TGFβ in alveolar development and pericyte migration and differentiation, we investigated the role of mesenchymal $G_{\alpha q/11}$ in a cyclical stretch model of TGFβ activation. Mesenchymal cells with and without intact $G_{\alpha q/11}$ signalling were subjected

to breathing-related CMS and TGFβ signalling was assessed. CMS-induced TGFβ signalling, as assessed by Smad2 phosphorylation, was significantly reduced in *Gnaq*$^{-/-}$*;Gna11*$^{-/-}$ MEFs compared with WT MEFs (**Figure 5A-B)**. This finding was specific to the $G_{\alpha q/11}$ family of G proteins, as there was no effect of $G_{\alpha 12/13}$ knockdown on stretch-induced TGFβ signalling in MEFs (**Figure 5A**).

To validate the role of $G_{\alpha q/11}$ in stretch-induced TGFβ signalling in mesenchymal cells across species, human lung fibroblasts (HLFs) with and without siRNA-induced *GNAQ* and *GNA11* knockdown were subjected to breathing-related CMS. *GNAQ* and *GNA11* siRNA led to substantial reductions in both $G_{\alpha q}$ and $G_{\alpha 11}$ protein expression in HLFs, and significantly reduced CMS-induced TGFβ signalling compared with scrambled control (Scr) siRNA as measured by phosphorylation of Smad2 (**Figure 5C-D**). These data indicate that $G_{\alpha q/11}$ is a key component of CMS-induced TGFβ signalling in both murine and human fibroblasts.

Previous studies have reported that $G_{\alpha q/11}$-induces TGFβ activation via the Rho-ROCK cascade and αv integrins in epithelial cells (Froese et al., 2016; Xu et al., 2009). As αvβ1, αvβ3, and αvβ5 integrins are expressed by myofibroblasts and are involved in TGFβ activation (Pakshir et al., 2020), we utilised chemical inhibition of these integrins and ROCK in our CMS model. When murine (**Figure 6A-B**) and human fibroblasts (**Figure 6C-D**) were subject to breathing-related CMS in the presence of the ROCK1/2 inhibitor, Y27632, CMS-induced TGFβ signalling was not reduced. Similarly, HLFs subject to CMS in the presence of a pan αv integrin inhibitor CWHM-12 (**Figure 6E-F**) or a β1 integrin-specific inhibitor (NOTT199SS) (**Figure 6G-H**) exhibited no reduction in CMS-induced Smad2 phosphorylation. These data imply a novel pathway for CMS-induced TGFβ signalling in mesenchymal cells which requires $G_{\alpha q/11}$, but is independent of ROCK and integrin signalling.

$G_{\alpha q/11}$ induces TGFβ2 production, which is then available for CMS-induced serine protease-mediated activation

Proteases can induce the activation of latent TGFβ independently of integrins, therefore we assessed the effect of protease inhibitors in our CMS-induced TGFβ signalling system. A pan serine protease inhibitor 4-(2-aminoethyl)benzenesulfonyl fluoride (AEBSF), decreased CMS-induced Smad2 phosphorylation in HLFs (**Figure 7A-B**), whereas the MMP inhibitor GM-6001 had no effect on CMS-induced TGFβ signalling even at high concentrations (**Figure 7C-D**). These findings indicate that serine proteases mediate CMS-induced TGFβ signalling in mesenchymal cells.

As TGFβ2 is the only TGFβ isoform that is not activated by integrins (Jenkins, 2008), we hypothesised that breathing-related CMS would predominantly activate the TGFβ2 isoform

in mesenchymal cells. While CMS did not influence TGFβ2 protein expression in HLFs, HLFs with siRNA-induced *GNAQ* and *GNA11* knockdown expressed less TGFβ2 than HLFs with intact $G_{\alpha q/11}$ signalling (**Figure 7E-F**), suggesting that $G_{\alpha q/11}$ plays a role in TGFβ2 production. Conversely, TGFβ1 protein expression was not affected by *GNAQ* and *GNA11* knockdown in HLFs (**Figure 7G**), suggesting that this is an isoform-specific effect.

To evaluate the role of this CMS-induced TGFβ2 signalling pathway in alveologenesis, we assessed TGFβ2 expression in the lungs of P14 mice. *Pdgfrb-Cre*$^{+/-}$*;Gnaq*$^{fl/fl}$*;Gna11*$^{-/-}$ lungs had a significantly lower TGFβ2 immunostaining score than *Gna11*$^{-/-}$ control lungs (**Figure 7I-J**). These data demonstrate that lungs lacking mesenchymal $G_{\alpha q/11}$ have less TGFβ2 available for breathing-related CMS-induced activation, and this may be important in alveologenesis in vivo.

Discussion

In this study, we used mice with a targeted deletion of $G_{\alpha q/11}$ in mesenchymal cells to demonstrate that mesenchymal $G_{\alpha q/11}$ is essential for normal alveolar development. Loss of $G_{\alpha q/11}$ mediated signalling in these cells is associated with a failure of the pericyte-to-myofibroblast transdifferentiation and myofibroblast synthetic function required for alveolar development. Using murine and human cells, we demonstrated that the mechanisms underlying this impaired pericyte and myofibroblast function is reduced mesenchymal cell TGFβ2 production. In the absence of mesenchymal $G_{\alpha q/11,}$ TGFβ2 is unavailable for activation by CMS-induced serine proteases thereby diminishing downstream TGFβ signalling in the developing lungs . These findings establish a previously undescribed role for breathing-related CMS in TGFβ2 activation, and implicate a role for TGFβ2 in alveolar development.

The role of $G_{\alpha q/11}$ in alveolar development has not previously been investigated, primarily because germline $G_{\alpha q/11}$ deletion is embryonically lethal (Offermanns et al., 1998) and murine alveolarisation occurs entirely postnatally (Beauchemin et al., 2016). Cell type-specific *Gnaq* and *Gna11* deletion in neural, cardiovascular, and haematological tissues have various manifestations ranging from no phenotype to profound cardiac abnormalities associated with perinatal death (Hoyer et al., 2010; Sassmann et al., 2010; Wettschureck et al., 2007; Wettschureck et al., 2004; Wettschureck et al., 2005; Wettschureck et al., 2001; Wettschureck et al., 2006). However, abnormalities of lung development have not been described in germline or conditional $G_{\alpha q/11}$ knockout mice. This suggests a unique role for mesenchymal $G_{\alpha q/11}$ in alveolar development.

We propose that the key mechanisms underlying the failure of normal alveologenesis in *Pdgfrb-Cre*$^{+/-}$*;Gnaq*$^{fl/fl}$*;Gna11*$^{-/-}$ mice are abnormalities in pericyte to myofibroblast differentiation and loss of myofibroblast synthetic function. This was evidenced by the existence of fewer lung parenchymal myofibroblasts in *Pdgfrb-Cre*$^{+/-}$*;Gnaq*$^{fl/fl}$*;Gna11*$^{-/-}$ lungs. Furthermore, *Pdgfrb-Cre*$^{+/-}$*;Gnaq*$^{fl/fl}$*;Gna11*$^{-/-}$ lungs contained reduced amounts of collagen and elastin compared with controls, and mesenchymal cells lacking $G_{\alpha q/11}$ express less *Col1a1*, *Col3a1*, and *Eln* mRNA than cells with intact $G_{\alpha q/11}$. As myofibroblasts induce secondary septation by depositing ECM proteins at the tips of developing secondary septae, these data suggest that mesenchymal $G_{\alpha q/11}$-induced myofibroblast differentiation and function are required for normal alveolar development.

In addition to abnormal myofibroblast differentiation from precursor cells, *Pdgfrb-Cre*$^{+/-}$*;Gnaq*$^{fl/fl}$*;Gna11*$^{-/-}$ mouse lungs also showed evidence of failed pericyte migration. *Pdgfrb-Cre*$^{+/-}$*;Gnaq*$^{fl/fl}$*;Gna11*$^{-/-}$ lungs contained abnormal peripheral pulmonary vessels, with a hypertrophic vascular smooth muscle layer. We hypothesise that pericyte $G_{\alpha q/11}$ deletion prevents pericytes from migrating away from the perivascular region to the alveolar parenchyma, resulting in dysregulated vascular smooth muscle growth. However, as the abnormal pulmonary vessels observed in *Pdgfrb-Cre*$^{+/-}$*;Gnaq*$^{fl/fl}$*;Gna11*$^{-/-}$ mice were similar to those seen in pulmonary arterial hypertension (PAH) (Patel et al., 2018), and disturbed GPCR signalling can increase hypoxia-induced pulmonary vascular remodelling (Cheng et al., 2012), *Pdgfrb-Cre*$^{+/-}$*;Gnaq*$^{fl/fl}$*;Gna11*$^{-/-}$ mice could have PAH secondary to hypoxia caused by abnormal alveolar architecture. *Pdgfrb-Cre*$^{+/-}$*;Gnaq*$^{fl/fl}$*;Gna11*$^{-/-}$ mice did not exhibit signs of respiratory distress at P14, and cardiac histology did not show evidence of right ventricular hypertrophy, which supports our hypothesis. However, firm conclusions on the cause of the abnormal peripheral pulmonary vessels in *Pdgfrb-Cre*$^{+/-}$*;Gnaq*$^{fl/fl}$*;Gna11*$^{-/-}$ mice cannot be drawn from this work, and this hypothesis requires further study.

As TGFβ drives pericyte to myofibroblast differentiation, pericyte migration, and ECM protein production (Harrell et al., 2018), we hypothesised that a defect in TGFβ activation occurs in *Pdgfrb-Cre*$^{+/-}$*;Gnaq*$^{fl/fl}$*;Gna11*$^{-/-}$ mice. Alveolarisation occurs entirely postnatally in mice, and it is at this stage of lung development when breathing-related CMS dramatically increases. Both lung stretch and TGFβ signalling are important for normal lung development (Donahoe et al., 2016), and CMS has been demonstrated to induce TGFβ signalling in a number of models and organ systems (Froese et al., 2016; Fujita et al., 2010; Furumatsu et al., 2013; John et al., 2016; Maeda et al., 2011; Russo et al., 2018; Wang et al., 2013). As the *Pdgfrb-Cre*$^{+/-}$*;Gnaq*$^{fl/fl}$*;Gna11*$^{-/-}$ mice were not fit for in vivo studies of CMS-induced TGFβ signalling, we established an in vitro method to test our hypothesis. Open access RNA-Seq data on the LungMAP and IPF Cell Atlas databases show that in human and mouse lung, PDGFRβ-

positive cells include pericytes, fibroblasts and myofibroblasts (www.ipfcellatlas.com; www.lungmap.net). We therefore used human lung fibroblasts and murine embryonic fibroblasts assess the role of mesenchymal $G_{\alpha q/11}$ in TGFβ signalling, and to demonstrate the generalisability of our findings across species.

Our data indicate a key role for mesenchymal $G_{\alpha q/11}$-mediated CMS-induced TGFβ activation in alveolar development. Using the same *Gnaq*$^{fl/fl}$;*Gna11*$^{-/-}$ mice used in the present work, John et al described a reduction in stretch-induced TGFβ signalling in the lungs of mice lacking $G_{\alpha q/11}$ in type II alveolar epithelial cells (John et al., 2016), supporting our conclusion. Furthermore, platelet-derived growth factor-β (*Pdgfrb*)-expressing cells are instrumental in injury-induced TGFβ activation in vivo (Henderson et al., 2013). However, contrary to previous work that reported that stretch-mediated TGFβ activation in whole lung slices and epithelial cells required αv integrins and ROCK signalling (Froese et al., 2016; Xu et al., 2009), our data suggest a novel pathway of CMS-induced TGFβ signalling in mesenchymal cells.

CMS-induced TGFβ signalling in mesenchymal cells was reduced by a serine protease inhibitor, suggesting that TGFβ2, an isoform that is activated by proteases but not integrins (Jenkins, 2008), may be the primary TGFβ isoform activated by mesenchymal cell stretch. $G_{\alpha q/11}$-deficient fibroblasts expressed less TGFβ2, but had unchanged levels of TGFβ1, compared with cells that express $G_{\alpha q/11}$, suggesting a TGFβ isoform-specific effect of $G_{\alpha q/11}$ deletion. $G_{\alpha q/11}$ therefore drives TGFβ2 production in fibroblasts, and mesenchymal $G_{\alpha q/11}$ deficiency may result in less TGFβ2 in the ECM available for protease-mediated activation.

TGFβ signalling is integral to several physiological processes, including the regulation of cellular proliferation and differentiation, and ECM homeostasis (Bartram and Speer, 2004). All three TGFβ isoforms are expressed at high levels during development with distinct spatial and temporal expression patterns (Schmid et al., 1991). The importance of tightly regulated TGFβ signalling in alveolar development is well established, with both over- and under-activity being implicated in disturbances to alveologenesis (Alejandre-Alcázar et al., 2008; Belcastro et al., 2015; Bonniaud et al., 2004; Chen et al., 2005; Chen et al., 2008; Deng et al., 2019; Gauldie et al., 2003; Nakanishi et al., 2007; Pieretti et al., 2014; Sterner-Kock et al., 2002; Vicencio et al., 2004). However, this is the first study to propose an isoform-specific role for TGFβ2 in mammalian alveolar development.

Tgfb2$^{-/-}$ mice die shortly after birth from a range of developmental defects that do not overlap with those seen in *Tgfb1*$^{-/-}$ or *Tgfb3*$^{-/-}$ mice (Kaartinen et al., 1995; Sanford et al., 1997; Shull et al., 1992). *Tgfb2*$^{-/-}$ mice have no gross lung morphological abnormalities in late intrauterine gestation, however collapsed conducting airways are found postnatally (Sanford

et al., 1997). Single cell RNA-Seq data from the LungMAP database suggests that *Tgfb2* mRNA expression peaks at P7 in mouse lung mesenchymal cells, a key time point when alveolar development is underway (Pozarska et al., 2017). While the *Pdgfrb-Cre*$^{+/-}$*;Gnaq*$^{fl/fl}$*;Gna11*$^{-/-}$ mice generated in the present study did not exhibit any of the developmental defects characteristic of*Tgfb2*$^{-/-}$ mice, it is possible that TGFβ2 production by non-mesenchymal cells types is sufficient to allow normal prenatal development. Additionally, as alveolarisation occurs entirely postnatally in mice, it is possible that TGFβ2 plays a role in alveolar development that could not be observed in *Tgfb2*$^{-/-}$ mice due to perinatal death.

An alternative explanation to an isoform-specific role for TGFβ2 in alveolar development is that the abnormal alveolar appearances observed in *Pdgfrb-Cre*$^{+/-}$*;Gnaq*$^{fl/fl}$*;Gna11*$^{-/-}$ mice occurs due to a reduction in overall TGFβ signalling. For example, *Tgfb2* deletion can reverse abnormalities in prenatal lung development associated with excessive TGFβ signalling (Dabovic et al., 2009). However, the non-overlapping phenotypes observed in *Tgfb1*$^{-/-}$, *Tgfb2*$^{-/-}$, and *Tgfb3*$^{-/-}$ mice, and the spatial- and temporal-specific expression patterns of each isoform in the developing lung (Pelton et al., 1990; Pelton et al., 1991; Schmid et al., 1991), suggest isoform-specific roles in lung development and support our hypothesis. What is clear is that loss of mesenchymal $G_{\alpha q/11}$ causes a loss of the precise control of TGFβ signalling in the lungs, resulting in abnormal alveologenesis.

The limitations of this study predominantly relate to the poor condition of *Pdgfrb-Cre*$^{+/-}$*;Gnaq*$^{fl/fl}$*;Gna11*$^{-/-}$ mice, which limited the analyses to a single time point and precluded the study of CMS in vivo. Furthermore, the growth restriction of *Pdgfrb-Cre*$^{+/-}$*;Gnaq*$^{fl/fl}$*;Gna11*$^{-/-}$ mice could have indicated a nutritional deficiency that could have contributed to delayed alveolar development. However, our in vitro data provide compelling evidence for a role for mesenchymal $G_{\alpha q/11}$ in a key lung developmental signalling pathway.

Furthermore, we propose that abnormalities in pericyte differentiation and migration underlie the defective alveologenesis observed in *Pdgfrb-Cre*$^{+/-}$*;Gnaq*$^{fl/fl}$*;Gna11*$^{-/-}$ mice, however the *Pdgfrb* gene is expressed by other cell types, including myofibroblasts, fibroblasts, and vascular smooth muscle cells (Henderson et al., 2013). While it is possible that disturbed TGFβ signalling in these cell types contributed to the lung phenotype in *Pdgfrb-Cre*$^{+/-}$*;Gnaq*$^{fl/fl}$*;Gna11*$^{-/-}$ mice, pericytes are major progenitors for all of these cell types, and are therefore likely to have played a primary role in the abnormalities observed.

In conclusion, this is the first study to generate mesenchymal $G_{\alpha q/11}$ deleted mice, and has demonstrated a novel signalling pathway for CMS-induced TGFβ2 signalling in murine embryonic and mature human mesenchymal cells that is important for alveologenesis.

These findings could have implications for the treatment of a number of conditions associated with dysregulated developmental pathways, including fibrosis, emphysema, and malignancy.

Acknowledgements

This work was funded by a Medical Research Council Clinical Research Training Fellowship held by ATG (MR P001327/1). ATG was also funded by National Institute for Health Research Academic Clinical Fellowship (2982) for part of this project. GJ is funded by an NIHR Research Professorship (NIHR-RP-2017-08-ST2-014). NCH is supported by a Wellcome Trust Senior Research Fellowship in Clinical Science (219542/Z/19/Z).

We thank Dr Thomas McInally (University of Nottingham, UK) and Dr David Griggs (St Louis University, Missouri, USA) for supplying the compounds NOTT199SS and CWHM-12, respectively. NOTT199SS was identified as part of an MSci Chemistry undergraduate integrin drug discovery collaboration between the School of Chemistry at the University of Nottingham and GlaxoSmithKline (GSK), supervised by Dr Simon Macdonald (GSK) and Dr Thomas McInally (University of Nottingham)

Author contributions

ATG and GJ conceived project. ATG performed experiments, conducted image analysis, and wrote the original draft manuscript. AEJ supervised and gave methodological guidance for mouse phenotyping experiments and microscopy. CJ performed TGFβ2 immunohistochemistry. ATG, AEJ, AH, and ALT conducted animal monitoring and tissue collection. ALT established original cultures of human lung fibroblasts used in this study. NCH and SO provided and guided the breeding of *Pdgfrb-Cre*$^{+/-}$ and *Gnaq*$^{fl/fl}$*;Gna11*$^{-/-}$ mice, respectively. GJ supervised the entire project. All authors reviewed the original draft manuscript and contributed to editing and preparation of the final manuscript.

Declarations of Interests

GJ reports grants from Astra Zeneca, grants from Biogen, personal fees from Boehringer Ingelheim, personal fees from Daewoong, personal fees from Galapagos, grants from Galecto, grants from GlaxoSmithKline, personal fees from Heptares, non-financial support from NuMedii, grants and personal fees from Pliant, personal fees from Promedior, non-financial support from Redx, personal fees from Roche, Trustee for Action for Pulmonary Fibrosis.

Figure titles and legends

Figure 1: *Pdgfrb-Cre$^{+/-}$;Gnaq$^{fl/fl}$;Gna11$^{-/-}$* mice are growth restricted

A) Genotype frequencies from *Pdgfrb-Cre$^{+/-}$* x *Gnaq$^{fl/fl}$;Gna11$^{-/-}$* breeding. Red line indicates the expected frequency for each genotype (30, 12.5%). Total n= 241, 24 litters, mean litter size 7.4. Chi-squared value (χ^2) = 22.03, degrees of freedom =7, $p<0.005$.

B) Body weights of P14 pups by genotype. Mean ± SEM, one way ANOVA with Tukey's multiple comparisons test, n = 12-43 per group

C) Photographs of a P14 pup with the *Pdgfrb-Cre$^{+/-}$; Gnaq$^{fl/fl}$; Gna11$^{-/-}$* genotype (left), and a *Gna11$^{-/-}$* littermate (right).

D) Body weights of all pups from *Pdgfrb-Cre / Gnaq$^{fl/fl}$; Gna11$^{-/-}$* crosses by sex at P14. Mean ± SEM, unpaired two-tailed Students T test, 88 female and 102 male mice.

Figure 2: *Pdgfrb-Cre$^{+/-}$;Gnaq$^{fl/fl}$;Gna11$^{-/-}$* mice have abnormal lung appearances characteristic of disturbed alveologenesis

A) Haematoxylin and eosin (H&E) (top), Ki67 immunohistochemistry (middle), and pro-SPC immunohistochemistry (bottom) staining of lungs from a P14 *Gna11$^{-/-}$* (left) and a *Pdgfrb-Cre$^{+/-}$;Gnaq$^{fl/fl}$;Gna11$^{-/-}$* mouse (right). Arrows on H&E images indicate secondary crests. Images representative of 4 mice per group. Scale bars show 100µm.

B) Mean linear intercept analysis of airspace size in P14 *Gna11$^{-/-}$* and *Pdgfrb-Cre$^{+/-}$;Gnaq$^{fl/fl}$;Gna11$^{-/-}$* mice. Median ± interquartile range, n=4 mice per group, two-tailed Mann Whitney test.

C) Alveolar wall thickness in P14 *Gna11$^{-/-}$* and *Pdgfrb-Cre$^{+/-}$;Gnaq$^{fl/fl}$;Gna11$^{-/-}$* mice. Median ± interquartile range, n=4 mice per group, two-tailed Mann Whitney test.

D) Quantification of the number of secondary crests per 20 x field in P14 *Gna11$^{-/-}$* and *Pdgfrb-Cre$^{+/-}$;Gnaq$^{fl/fl}$;Gna11$^{-/-}$* mice. Median ± interquartile range, n=4 mice per group, two-tailed Mann Whitney test.

E) Quantification of Ki67 immunohistochemistry in P14 *Gna11$^{-/-}$* and *Pdgfrb-Cre$^{+/-}$;Gnaq$^{fl/fl}$;Gna11$^{-/-}$* mice. Shown as the percentage of Ki67 positive nuclei per 40x magnification field. Median ± interquartile range, n=4 mice per group, two-tailed Mann Whitney test.

F) Quantification of Pro-SPC immunohistochemistry in P14 *Gna11*$^{-/-}$ and *Pdgfrb-Cre*$^{+/-}$*;Gnaq*$^{fl/fl}$*;Gna11*$^{-/-}$ mice. Shown as the percentage of pro-SPC positive cells per 40x magnification field. Median ± interquartile range, n=4 mice per group, two-tailed Mann Whitney test.

G) Relative lung weights compared with body weights in P14 *Gna11*$^{-/-}$ and *Pdgfrb-Cre*$^{+/-}$*;Gnaq*$^{fl/fl}$*;Gna11*$^{-/-}$ mice. Median ± interquartile range, n=5-6 mice per group, two-tailed Mann Whitney test.

Figure 3: *Pdgfrb-Cre*$^{+/-}$*;Gnaq*$^{fl/fl}$*;Gna11*$^{-/-}$ mice have reduced lung myofibroblast differentiation and function

A) αSMA immunohistochemistry (top), elastin staining (second row), and picrosirius red (PSR) staining (row 3-5) from P14 *Gna11*$^{-/-}$ (left) and *Pdgfrb-Cre*$^{+/-}$*;Gnaq*$^{fl/fl}$*;Gna11*$^{-/-}$ (right) mice. Arrows on elastin images shown elastin fibres. Picrosirius red images shown are bright field (BF, third row), polarised light (fourth row), and bright field at high magnification (fifth row). Representative images from 4 mice per genotype. Scale bars show 100μm (αSMA, PSR), 50μm (elastin), and 10μm (picrosirius red high magnification).

B) Quantification of the proportion of secondary crests that stained positively for αSMA in P14 *Gna11*$^{-/-}$ and *Pdgfrb-Cre*$^{+/-}$*;Gnaq*$^{fl/fl}$*;Gna11*$^{-/-}$ lungs. Median ± interquartile range, n=4 mice per group, two-tailed Mann Whitney test.

C) *Acta2* mRNA expression in WT, *Gna12*$^{-/-}$*;Gna13*$^{-/-}$, and *Gnaq*$^{-/-}$*;Gna11*$^{-/-}$ MEFs. Median ± interquartile range, n=4 per group, two-tailed Mann Whitney test.

D) Representative western blot showing αSMA expression in wild-type (WT), *Gna12*$^{-/-}$*;Gna13*$^{-/-}$, and *Gnaq*$^{-/-}$*;Gna11*$^{-/-}$ MEFs.

E) Densitometry of western blots of αSMA expression in wild-type (WT), *Gna12*$^{-/-}$*;Gna13*$^{-/-}$, and *Gnaq*$^{-/-}$*;Gna11*$^{-/-}$ MEFs. Median ± interquartile range, n=4, two-tailed Mann Whitney test.

F) The number of elastin fibres per high powered field (40 x magnification) in P14 *Gna11*$^{-/-}$ and *Pdgfrb-Cre*$^{+/-}$*;Gnaq*$^{fl/fl}$*;Gna11*$^{-/-}$ lungs. Median ± interquartile range, n=4 mice per group, two-tailed Mann Whitney test.

G) The proportion of secondary crests that stained positively for elastin in each high powered field (40 x magnification) in P14 *Gna11*$^{-/-}$ and *Pdgfrb-Cre*$^{+/-}$*;Gnaq*$^{fl/fl}$*;Gna11*$^{-/-}$ lungs. Median ± interquartile range, n=4 mice per group, two-tailed Mann Whitney test.

H) *Eln* mRNA expression in wild-type (WT) and *Gnaq*$^{-/-}$;*Gna11*$^{-/-}$ MEFs. Median ± interquartile range, n=4, two-tailed Mann Whitney test.

I) *Col1a1* mRNA expression in wild-type (WT) and *Gnaq*$^{-/-}$;*Gna11*$^{-/-}$ MEFs. Median ± interquartile range, n=4, two-tailed Mann Whitney test.

J) *Col3a1* mRNA expression in wild-type (WT) and *Gnaq*$^{-/-}$;*Gna11*$^{-/-}$ MEFs. Median ± interquartile range, n=4, two-tailed Mann Whitney test.

Figure 4: The lungs of *Pdgfrb-Cre*$^{+/-}$;*Gnaq*$^{fl/fl}$;*Gna11*$^{-/-}$ mice contain abnormal peripheral pulmonary vessels.

Lung sections from P14 *Pdgfrb-Cre*$^{+/-}$;*Gnaq*$^{fl/fl}$;*Gna11*$^{-/-}$ mice were stained using various techniques.

A) Haematoxylin and eosin stain. Scale bar shows 100µm.
B) Verhoeff van Gieson stain for Elastin. Scale bar shows 50µm.
C) Picrosirius red stain (PSR). Same image shown using bright field (BF, left) and polarised light (PL, right) illumination). Scale bar shows 20µm.
D) CD31 immunohistochemistry. Scale bar shows 10µm.
E) αSMA immunohistochemistry. Scale bar shows 10µm.
F) Ki67 immunohistochemistry. Scale bar shows 10µm.
G) Quantification of maximum peripheral vessel wall thickness in P14 *Gna11*$^{-/-}$ and *Pdgfrb-Cre*$^{+/-}$;*Gnaq*$^{fl/fl}$;*Gna11*$^{-/-}$ lungs. Median ± interquartile range, n=4 mice per group, two-tailed Mann Whitney test.
H) Quantification of minimum peripheral vessel wall thickness in P14 *Gna11*$^{-/-}$ and *Pdgfrb-Cre*$^{+/-}$;*Gnaq*$^{fl/fl}$;*Gna11*$^{-/-}$ lungs. Median ± interquartile range, n=4 mice per group, two-tailed Mann Whitney test.

Figure 5: $G_{\alpha q/11}$ mediates stretch-induced TGFβ signalling in murine and human fibroblasts

A) Representative western blot showing pSmad2 expression in wild-type (WT), *Gna12*$^{-/-}$;*Gna13*$^{-/-}$, and *Gnaq*$^{-/-}$*Gna11*$^{-/-}$ MEFs subject to cyclical stretch (15% elongation, 1Hz, 48 hours).
B) Densitometry of western blots from stretched MEFs shown as pSmad2 relative to Smad2 expression from 4 independent experiments. Median ± interquartile range, n=4, two-tailed Mann Whitney Test.
C) Representative western blot showing pSmad2 expression in HLFs treated with non-targeting (Scr) or *GNAQ* and *GNA11* siRNA then subject to cyclical stretch (15% elongation, 0.3Hz, 24 hours).

D) Densitometry of western blots from stretched HLFs shown as pSmad2 relative to Smad2 expression from 4 independent experiments. Median ± interquartile range, n=4, two-tailed Mann Whitney Test.

+ = stretched; - = unstretched

Figure 6: Cyclical stretch-induced TGFβ activation occurs independently of ROCK, and αv and β1 integrins in fibroblasts.

A) Representative pSmad2 western blot of wild type MEFs treated with the ROCK1/2 inhibitor Y27632 then subject to 48 hours of cyclical stretch (15% elongation, 1Hz, 48 hours).
B) Relative pSmad2 to Smad2 densitometry from western blots of wild-type MEFs treated with Y27632 then subject to cyclical stretch. Median ± interquartile range, n=4, two-tailed Mann Whitney test.
C) Representative pSmad2 western blot of human lung fibroblasts treated with Y27632 then subject to 48 hours of cyclical stretch (15% elongation, 0.3Hz, 48 hours).
D) Relative pSmad2 to Smad2 densitometry from western blots of human lung fibroblasts treated with Y27632 then subject to cyclical stretch. Median ± interquartile range, n=4, two-tailed Mann Whitney test.
E) Representative pSmad2 western blot of human lung fibroblasts treated with an αv integrin inhibitor (CWHM-12) then subject to 48 hours of cyclical stretch (15% elongation, 0.3Hz, 48 hours).
F) Relative pSmad2 to Smad2 densitometry of human lung fibroblasts treated with CWHM-12 then subject to cyclical stretch. Median ± interquartile range, n=4, two-tailed Mann Whitney test.
G) Representative pSmad2 western blot of human lung fibroblasts treated with a β1 integrin inhibitor (NOTT199SS) then subject to 48 hours of cyclical stretch (15% elongation, 0.3Hz, 48 hours).
H) pSmad2 relative to Smad2 densitometry of human lung fibroblasts treated with NOTT199SS then subject to cyclical stretch. Median ± interquartile range, n=4, two-tailed Mann Whitney Test.

+ = stretched; - = unstretched. Alk5 inh = 50μM Alk5 inhibitor (SB525334)

Figure 7: $G_{\alpha q/11}$ signalling induces the production of TGFβ2 which is then available for stretch-induced serine protease-mediated activation

A) Representative pSmad2 western blot of human lung fibroblasts treated with the serine protease inhibitor AEBSF then subject to cyclical stretch (15% elongation, 0.3Hz, 48 hours).

B) Relative pSmad2 to Smad2 densitometry of human lung fibroblasts treated with AEBSF then subject to cyclical stretch. Median ± interquartile range, n=4, two-tailed Mann Whitney test.

C) Representative pSmad2 western blot of human lung fibroblasts treated with the matrix metalloproteinase inhibitor GM6001 then subject to cyclical stretch (15% elongation, 0.3Hz, 48 hours).

D) Relative pSmad2 to Smad2 densitometry from human lung fibroblasts treated with GM6001 then subject to cyclical stretch. Median ± interquartile range, n=4, two-tailed Mann Whitney test.

E) Representative TGFβ2 western blot of human lung fibroblasts subject to non-targeting (Scr) or *GNAQ* and *GNA11* siRNA and cyclical stretch (15% elongation, 0.3Hz, 24 hours).

F) Relative TGFβ2 to GAPDH densitometry of human lung fibroblasts with and without siRNA-induced *GNAQ* and *GNA11* knockdown. Median ± interquartile range, n=4, two-tailed Mann Whitney test

G) Representative TGFβ1 western blot of human lung fibroblasts subject to non-targeting (Scr) or *GNAQ* and *GNA11* siRNA and cyclical stretch (15% elongation, 0.3Hz, 24 hours).

H) Relative TGFβ1 to GAPDH densitometry of human lung fibroblasts with and without siRNA-induced *GNAQ* and *GNA11* knockdown. Median ± interquartile range, n=4, two-tailed Mann Whitney test.

I) TGFβ2 immunohistochemistry on P14 *Gna11*$^{-/-}$ (left) and *Pdgfrb-Cre*$^{+/-}$ *;Gnaq*$^{fl/fl}$*;Gna11*$^{-/-}$ (right) mouse lungs.

J) TGFβ2 immunohistochemistry scores of P14 *Gna11*$^{-/-}$ (left) and *Pdgfrb-Cre*$^{+/-}$ *;Gnaq*$^{fl/fl}$*;Gna11*$^{-/-}$ (right) mouse lungs. Median ± interquartile range, n=4, two-tailed Mann Whitney test.

+ = stretched; - = unstretched.

STAR methods

Resource Availability

Lead Contact

Further information and requests for resources and reagents should be directed to and will be fulfilled by the Lead Contact, Amanda Goodwin (Amanda.Goodwin@nottingham.ac.uk).

Materials Availability

This study did not generate new unique reagents.

Data and Code Availability

This study did not analyse or generate any new datasets or code

Experimental Model and Subject Details

Animal Studies

Husbandry

Mice were housed under specific pathogen-free conditions, with standard food and water available *ad libitum*. All animal experiments were performed in accordance with the Animals (Scientific Procedures) Act 1986, and approved by the Animal Welfare and Ethical Review Board at the University of Nottingham.

Breeding strategy

Mice with floxed alleles for *Gnaq* and germline deficiency in *Gna11* (*Gnaq*$^{fl/fl}$;*Gna11*$^{-/-}$) were crossed with mice that express Cre recombinase under the control of the *Pdgfrb* gene

(*Pdgfrb-Cre*$^{+/-}$). *Pdgfrb-Cre*$^{+/-}$;*Gnaq*$^{+/fl}$;*Gna11*$^{+/-}$ offspring from this F1 generation were then bred with *Gnaq*$^{fl/fl}$;*Gna11*$^{-/-}$ founders to produce an F2 generation, including *Pdgfrb-Cre*$^{+/-}$;*Gnaq*$^{fl/fl}$;*Gna11*$^{-/-}$ mice. The genetic background for all mice was predominantly C57BL6, with a minimum of a six backcross generations. The generation of *Gnaq*$^{fl/fl}$;*Gna11*$^{-/-}$ and *Pdgfrb-Cre*$^{+/-}$ mice has been described previously (Foo et al., 2006; Offermanns et al., 1998; Wettschureck et al., 2001).

Genotyping

Mice were genotyped using DNA isolated from ear notch biopsies by PCR analysis with allele-specific primers. Primer sequences: *Cre* transgene 5'- GCG GTC TGG CAG TAA AAA CTA TC – 3', 5' - GTG AAA CAG CAT TGC TGT CAC TT – 3' (product 100bp); internal positive control 5' - CTA GGC CAC AGA ATT GAA AGA TCT – 3', 5' - GTA GGT GGA AAT TCT AGC ATC ATC C – 3' (product 324bp); *Gna11* wild-type 5' – AGC ATG CTG TAA GAC CGT AG - 3', 5' – GCC CCT TGT ACA GAT GGC AG – 3' (product 820bp); *Gna11* knockout 5' - CAG GGG TAG GTG ATG ATT GTG – 3', 5' – GAC TAG TGA GAC GTG CTA CTT CC - 3' (product 450bp); *Gnaq* wild-type and floxed alleles 5' – GCA TGC GTG TCC TTT ATG TGA G 3', 5' – AGC TTA GTC TGG TGA CAG AAG – 3' (products: 600bp (wild type), 700bp (floxed).

PCR products were analysed by electrophoresis on ethidium bromide-stained agarose gels.

Mice were genotyped at 2 weeks old (P14). Genotype ratios of F2 mice from the *Gnaq*$^{fl/fl}$;*Gna11*$^{-/-}$ and *Pdgfrb*$^{+/-}$ crosses were compared with the expected Mendelian frequency (12.5% per genotype).

Human Cells

For in vitro experiments using human lung fibroblasts, cells from 4-6 donors were used per group. Cells were used at passage 5-6 for all in vitro experiments.

Human lung fibroblasts (HLFs) were isolated from donated post-mortem or surgical lung biopsy samples, from male and female donors with and without pulmonary fibrosis. For non-fibrotic fibroblasts, cells were isolated from regions of lung distant from the area of primary diagnosis. Tissue was cut into 1mm x 1mm pieces and placed 10mm apart in a 10cm cell culture dish. Tissue was cultured in DMEM supplemented with 10% foetal calf serum (FCS, Fisher), L-glutamine (4mM, Sigma), penicillin (200 units/ml, Sigma), streptomycin (0.2mg/ml, Sigma), and amphotericin B (2.5µg/ml). Fibroblast outgrowth could be seen after 6-8 days. Tissue was removed from the cell culture dish if it became detached, or when cells had

reached 80% confluency and were ready for passage. Cells were maintained in a humidified incubator at 37^{o}C, 5% CO_2/ 95% air, in Dulbecco's Modified Eagle's Medium (DMEM, Sigma), supplemented with 10% foetal calf serum (FCS, Fisher), L-glutamine (4mM, Sigma), penicillin (100 units/ml, Sigma) and streptomycin (0.1mg/ml, Sigma).

Murine Cells

Wild-type, *Gna12*$^{-/-}$*;Gna13*$^{-/-}$, and *Gnaq*$^{-/-}$*;Gna11*$^{-/-}$ murine embryonic fibroblasts (MEFs) were a gift from Dr Stefan Offermanns, and their generation has been described elsewhere (Gu et al., 2002; Zywietz et al., 2001). Cells were maintained in a humidified incubator at 37^{o}C, 5% CO_2/ 95% air, in Dulbecco's Modified Eagle's Medium (DMEM, Sigma), supplemented with 10% foetal calf serum (FCS, Fisher), L-glutamine (4mM, Sigma), penicillin (100 units/ml, Sigma) and streptomycin (0.1mg/ml, Sigma).

Method details

Mouse studies

Mouse Phenotyping

Litters were observed for signs of ill health daily from birth. Mice were weighed at P14. Male and female mice were included in all analyses. Mice had not undergone any previous procedures. Mouse phenotyping analyses were performed by an observer blinded to genotype.

Mouse Organ Collection

Mice were humanely killed by intraperitoneal injection of pentobarbital at P14, and organs collected for histological analyses. The lungs were perfused by injecting 40units/ml heparin sodium in PBS (Wockhardt) into the right ventricle, and inflated by cannulating the trachea and filling the lungs with 10% formalin (VWR) under gravity. The trachea was ligated, and the heart and lungs removed en bloc. Organs were kept in 10% formalin (VWR) for 24 hours before paraffin embedding and sectioning.

Tissue histology staining

3µm (lung), and 5µm (heart) formalin-fixed paraffin embedded tissue sections were deparaffinised in xylene and rehydrated in graded alcohols. Haematoxylin and eosin, Verhoeff van Gieson (elastin), and picrosirius red staining were performed as per standard protocols using buffers and stains prepared in house and mounted in DPX.

Staining solutions made in house

The following histology solutions were generated in house: Weigert's iodine (2g potassium iodide, 1g iodine, 100ml distilled water); Verheoff's solution (20ml 5% alcoholic haematoxylin, 8ml 10% ferric chloride, 8ml Weigert's iodine); Van Gieson's solution (5ml aqueous acid fuschin, 100ml saturated aqueous picric acid); Picro-sirius red solution (0.5g Direct Red 80 (Sigma), 500ml saturated aqueous picric acid); Weigert's haematoxylin (1:1 ratio of Weigert's solution A and Weigert's solution B); Weigert's solution A (1% haematoxylin in 100% ethanol); Weigert's solution B (4ml 30% ferric chloride, 1ml 12N hydrochloric acid, 95ml water); Acidified water (5ml glacial acetic acid, 1l distilled water); Acid/alcohol solution (70% ethanol, 0.1% hydrochloric acid).

Haematoxylin and eosin (H&E) stain

After being deparaffinised and rehydrated, tissue sections were submerged in Mayers haematoxylin (Fisher) for 2 minutes, acid/alcohol solution for 1 minute, then 1% eosin solution (VWR) for 3 minutes. Sections were rinsed with tap water between each step, then dehydrated and mounted.

Elastin (Verhoeff Van Gieson) stain

Lung sections were deparaffinised and hydrated to distilled water, then stained in Verhoeff's solution for 1 hour until the tissue was completely black. Sections were differentiated in 2% ferric chloride until elastin fibres were seen on a grey background, incubated in 5% sodium thiosulphate for 1 minute, and then washed in running tap water for 5 minutes. Sections were then counterstained in Van Gieson's solution for 5 minutes, dehydrated and mounted as above.

Picrosirius red stain

Lung, kidney, and heart sections were deparaffinised and hydrated. Nuclei were stained with Weigert's haematoxylin for 8 minutes, and then washed in running tap water for 5 minutes. Sections were incubated in picrosirius red for 1 hour, washed in two changed of acidified water, then dehydrated and mounted.

Immunostaining

Tissue sections were deparaffinised in xylene and rehydrated in graded alcohols. Heat-mediated antigen retrieval was performed by boiling sections in a microwave for 20 minutes in 10mM citric acid buffer (pH 6.0). Endogenous peroxidase activity was blocked by incubating sections in 3% hydrogen peroxide in methanol for 30 minutes. Nonspecific

binding was blocked with 5% goat serum (Sigma) in 0.1% BSA/PBS. Sections were incubated with primary antibody in 5% goat serum overnight at 4^{o}C in a humidified chamber, followed by incubations for 60 minutes with secondary antibody and 30 minutes with avidin-biotin complex (Vector). Sections were then stained with diaminobenzidine (Sigma), counterstained with Mayers haematoxylin (Sigma), and mounted in DPX (Sigma). Slides were washed in PBS (Sigma) between incubation steps.

The following antibodies were used for immunohistochemistry: Rabbit anti-αSMA (Abcam, ab5694; 1:500), rabbit anti-CD31 (Abcam, ab182981; 1:2000), rabbit anti-ki67 (Abcam, ab15580; 1µg/ml), rabbit anti-pro-surfactant protein C (Sigma, Ab3786; 1:2000), rabbit anti-TGFβ2 (Proteintech, 19999-1-AP; 1:3000), and biotinylated goat anti-rabbit IgG (Vector, BA1000; 1:200).

Image Quantification

Image acquisition

Images of H&E, elastin, and IHC were taken using a Nikon 90i microscope and NIS-Elements software v3.2 (Nikon). Polarised light imaging of picrosirius red stained samples was performed using a Zeiss Axioplan microscope (Zeiss) and MicroManager 1.4 software (Vale Lab, UCSF).

Staining quantification

For all analyses of histology images, *Pdgfrb-Cre*$^{+/-}$ *;Gnaq*$^{fl/fl}$*;Gna11*$^{-/-}$ mice were compared with *Pdgfrb-Cre*$^{-/-}$*;Gnaq*$^{fl/fl}$*;Gna11*$^{-/-}$ littermate controls (labelled as *Gna11*$^{-/-}$ controls). For histological analyses, four animals per genotype were assessed to allow differences in histological appearances to be detected. All image quantification was performed by an observer blinded to genotype.

For quantitative analyses, 5-10 images were assessed per set of lungs, covering all lobes and avoiding major airways and central blood vessels. All morphometric analyses were performed using NIS Elements software v3.2 (Nikon), with the exception of peripheral pulmonary vessel thickness measurements, which were performed using CaseViewer 2.3 software (3D Histech).

For quantification of immunohistochemistry and elastin staining, the “count” feature of ImageJ (NIH) was used. Elastin fibres were identified as thin black fibres, and secondary crests were elastin positive if they had black staining that was not clearly a cell nucleus on

Verhoeff van Geison staining. For immunohistochemistry staining, a cell was counted if it stained brown. Only nuclear DAB staining was counted for Ki67 quantification. For αSMA quantification, the number of αSMA-positive secondary crests per 40 x field was counted. For Ki67 and pro-SPC staining, the total number of cells per 40x field was quantified by counting nuclei, and the proportion of Ki67 or pro-SPC positive cells calculated by dividing the number of stained cells per image by the total number of cells per image.

For quantification of TGFβ2 staining, the following scoring system was used and 7 fields (20x magnification) per mouse were analysed:

- **Score 0**: No cells stained.
- **Score 0.5**: 1-25 cells stained at low intensity
- **Score 1.0**: 1-25 cells stained at high intensity
- **Score 1.5**: 26-50 cells stained at low intensity
- **Score 2.0**: 26-50 cells stained at high intensity
- **Score 2.5**: >50 cells stained at low intensity
- **Score 3.0**: >50 cells stained at high intensity

Morphometry

Mean linear intercept (MLI) analysis of airspace size was performed as previously described (John et al., 2016). Briefly, 10x magnification images were overlaid with a grid comprised of 100µm squares, and “intercepts” between gridlines and airspace walls counted. The MLI was calculated by dividing the length of each gridline was divided by the intercept count. For alveolar wall thickness measurements, 40x magnification images were overlaid with five equally spaced horizontal lines and the alveolar wall thickness measured at points where lung tissue crossed each line using the “measure” function of NIS Elements. Mean MLI and alveolar wall thickness values were calculated for each mouse from all measurements across all images and data presented as median ± interquartile range. For secondary crest counts, 10x magnification images were used and secondary crests counted for each image. For peripheral vessel wall thickness, ten random peripheral pulmonary vessels were identified using CD31 staining. Maximal and minimum vessel wall thickness in µm was measured using the “measure” function of CaseViewer. For assessment of right ventricular hypertrophy, the left and right cardiac ventricular wall thickness was measured using CaseViewer, and the right: left ventricular wall thickness ratio calculated.

Breathing-related cyclical stretch experiments

Cells were seeded at 2 x 10^5 cells per well on collagen I-coated Bioflex® 6 well culture plates (Dunn Labortechnik) in DMEM supplemented with 10% FCS, L-glutamine (4mM), penicillin (100 units/ml) and streptomycin (0.1mg/ml) and allowed to adhere for 24 hours. The culture medium was changed to 1% FCS in DMEM with 4mM L-glutamine for 24 hours before stretching commenced. The Flexcell® FX-5000T system (Flexcell International Corporation) was used to apply cyclical stretch to cells in vitro, according to the manufacturer's instructions. MEFs were stretched at a frequency of 1Hz, and HLFs at 0.3Hz in order to mimic breathing in the relevant organism. 15% elongation and a sine waveform were used for all cyclical stretch experiments. Cyclical stretch was applied for 48 hours, except for experiments using siRNA-induced *GNAQ* and *GNA11* knockdown, where 24 hours of cyclical stretch was used. Unstretched control cells were cultured in identical conditions alongside the Flexcell® apparatus. Cells were lysed in protein lysis buffer (Cell Signalling) supplemented with phosphatase (Phos-Stop, Sigma) and protease (Complete Mini, Sigma) inhibitors, and 20µM PMSF. All experimental replicates were performed independently.

Chemical Inhibitors used in Cyclical Stretch System

When used, inhibitor compounds were applied in DMEM supplemented with 1% FCS and 4mM L-glutamine 30 minutes before stretching commenced. The activin receptor-like kinase (ALK5)/ type I TGFβ-receptor kinase inhibitor SB-525334 (Sigma) was used at a concentration of 50µM. A ROCK inhibitor (Y27632, Sigma), pan-αv integrin inhibitor (CWHM-12), β1 integrin inhibitor (NOTT199SS) matrix metalloproteinase (MMP) inhibitor GM6001 (Sigma), and serine protease inhibitor AEBSF (Sigma) were used at varying concentrations. Where inhibitors were dissolved in DMSO, the negative control cells were treated with a DMSO concentration equivalent to that used in the highest inhibitor concentration.

GNAQ and GNA11 siRNA

SiRNAs for human *GNAQ* (Dharmacon ON-TARGET-plus SMARTpool GNAQ) and *GNA11* (Dharmacon ON-TARGET-plus SMARTpool GNA11) were used to induce *GNAQ* and *GNA11* knockdown. A non-targeting siRNA pool was used as a control (Dharmacon ON-TARGET-plus non-targeting pool).

Cells were seeded at 1.5 x 10^5 cells per well of a 6 well Flexcell® plate in antibiotic-free DMEM supplemented with 10% FCS and 4mM L-glutamine. The following day, *GNAQ* and *GNA11* siRNA was applied at a concentration of 15nM each with 4µl/ml DharmaFECT 1

transfection reagent (Dharmacon) as per the manufacturer's protocol. At 48 hours after transfection, the media was changed to DMEM supplemented with 1% FCS and 4mM L-glutamine. Cyclical stretch was applied for 24 hours from 72 hours post-transfection. LPA stimulation was applied for 4 hours from 72 hours post-transfection. $G_{\alpha q/11}$ knockdown was confirmed by western blot and qPCR

Western blotting

Protein concentrations were determined by BCA assay using a commercially available kit (ThermoFisher), according to the manufacturer's instructions. Equal amounts of protein (15-25µg) were loaded per lane of a 10% SDS-polyacrylamide gel and subject to electrophoresis, and transferred onto a polyvinylidene fluoride membrane (BioRad). Membranes were blocked for 1 hour in either 5% non-fat milk (pSmad2, Smad2/3, αSMA, $G_{\alpha q}$, $G_{\alpha 11}$, GAPDH) or 3% BSA (TGFβ1, TGFβ2) in tris-buffered saline containing 0.1% Tween, pH 7.4 (TBST). Membranes were incubated overnight at 4^{O}C in blocking buffer with the appropriate primary antibody. Membranes were washed in TBST, then incubated for 1-2 hours in the appropriate HRP-conjugated secondary antibody in blocking buffer. Western blots were analysed using chemilluminescence and exposure to film (GE Healthcare). Where membranes were probed for two different proteins of the same molecular weight, i.e. pSmad2 and Smad2, the membrane was stripped after analysis of pSmad2 using Western Restore Stripping Buffer (Thermo-Fisher) for 5 minutes and re-blocked with 5% non-fat milk before application of the second primary antibody.

The following antibodies were used for western blots: Rabbit anti-phospho-Smad2 (pSmad2) (Cell Signaling Technology, 3808; 1:1000), rabbit anti-Smad2/3 (Cell Signaling Technology, 3102; 1:1000), rabbit anti-αSMA (Abcam, ab5694; 0.5µg/ml), rabbit anti-GAPDH (Abcam, ab181603; 1:10,000), rabbit anti-TGFβ1 (ab92486; 4µg/ml), mouse anti-TGFβ2 (Abcam, ab36495; 1:1000), rabbit anti $G_{\alpha 11}$ (Abcam, ab153951; 1:1000), goat anti-$G_{\alpha q}$ (Abcam, ab128060; 0.1µg/ml), HRP-conjugated goat-anti-rabbit (Agilent, P044801-2; 1:3000), HRP-conjugated rabbit-anti-goat (Agilent, P016002-2; 1:3000), HRP-conjugated rabbit anti-mouse (Agilent, P0260022-2, 1:3000).

Densitometry Analysis of Western Blots

Densitometry was performed using ImageJ (NIH) on scanned western blot images. JPEG images were converted into greyscale images, and the software used to calculate densitometry values for each band relative to the other bands. These relative densitometry

values were used to calculate the expression of protein relative to loading control using the equation: Protein relative to loading control = protein densitometry value/ loading control protein densitometry value

Quantitative PCR

RNA was isolated from in vitro experiments using the Machery-Nagel Nucleospin RNA isolation kit according to the manufacturer's instructions. Complementary DNA (cDNA) was reverse transcribed from 200µg RNA using Superscript IV Reverse Transcriptase (Thermo Fisher) according to the manufacturer's protocol. Quantitative PCR was performed on cDNA using gene-specific primers (see below), KAPA SYBR FastTaq (Sigma), and MXPro3000 qPCR machine (Stratagene) at an annealing temperature of 60°C for 40 cycles. Amplification of a single PCR product was confirmed by melting curve analysis. The delta-delta Ct method was used to quantify gene expression relative to the housekeeping genes *Hprt* (mouse samples) or *B2M* (human samples).

Primer sequences for mouse genes were: *Hprt* forward 5' – TGA AAG ACT TGC TCG AGA TGT CA - 3', *Hprt* reverse 5' – CCA GCA GGT CAG CAA AGA ACT 3', *Acta2* forward 5' - GGG ATC CTG ACG CTG AAG TA – 3', *Acta2* reverse 5' – GAC AGC ACA GCC TGA ATA GC – 3', *Eln* forward 5' GAT GGT GCA CAC CTT TGT TG 3', *Eln* reverse 5' CAG TGT GAG GAG CCA TCT CA 3', *Col1a1* forward 5' AGC TTT GTG CAC CTC CGG CT 3', *Col1a1* reverse 5' ACA CAG CCG TGC CAT TGT GG 3', *Col3a1* forward 5' TTT GCA GCC TGG GCT CAT TT 3', *Col3a1* reverse 5' AGG TAC CGA TTT GAA CAG ACT

Primer sequences for human genes were: *GNAQ* forward 5' – GGACAGGAGAGGGTGGCAAG – 3', *GNAQ* reverse 5' – TGGGATCTTGAGTGTGTCCA – 3', *GNA11* forward 5' – CCACTGCTTTGAGAACGTGA – 3', *GNA11* reverse 5' GCAGGTCCTTCTTGTTGAGG – 3', *B2M* forward 5'AATCCAAATGCGGCATCT3', *B2M* reverse 5'GAGTATGCCTGCCGTGTG3'.

Statistical Analyses

Statistical analyses were performed using GraphPad Prism 8.2 software (GraphPad). For experiments with group sizes of 5 or less, a non-parametric test was used. For experiments with group sizes of 6 or over, data were assessed for normality and a parametric test used if data followed a normal distribution.

Key Resources Table

REAGENT or RESOURCE	SOURCE	IDENTIFIER
Antibodies		
Rabbit anti-phospho-Smad2 (pSmad2)	Cell Signaling Technology	Cat# 3808L
Rabbit anti-Smad2/3	Cell Signaling Technology	Cat# 3102
Rabbit anti-α-smooth muscle actin (αSMA)	Abcam	Cat# ab5694
Rabbit anti-GAPDH	Abcam	Cat# ab181603
Rabbit anti-TGFβ1	Abcam	Cat# ab92486
Mouse anti-TGFβ2	Abcam	Cat# ab36495
Rabbit anti $G_{\alpha 11}$	Abcam	Cat# ab153951
Goat anti-$G_{\alpha q}$	Abcam	Cat# ab128060
HRP-conjugated goat-anti-rabbit	Agilent	Cat# P044801-2
HRP-conjugated rabbit-anti-goat	Agilent	Cat# P016002-2
HRP-conjugated rabbit anti-mouse	Agilent	Cat# P0260022-2
Rabbit anti-CD31	Abcam	Cat# ab182981
Rabbit anti-ki67	Abcam	Cat# ab15580
Rabbit anti-pro-surfactant protein C	Sigma	Cat# Ab3786
Rabbit anti-TGFβ2	Proteintech	Cat# 19999-1-AP
Biotinylated goat anti-rabbit IgG	Vector	Cat# BA1000
Chemicals, Peptides, and Recombinant Proteins		
Protein lysis buffer	Cell Signaling Technology	Cat# 9803
Phos-stop phosphatase inhibitors	Sigma	Cat# 04906837001
Complete mini protease inhibitors	Sigma	Cat# 04693124001
PMSF	Sigma	Cat# P7626
SB-525334 (ALK5 inhibitor)	Sigma	Cat# S8822

Y27632 (ROCK inhibitor)	Sigma	Cat# Y0503
CWHM-12 (αv integrin inhibitor)	A gift from Dr David Griggs, University of St Louis. Now commercially available from various suppliers	https://www.medchemexpress.com/CWHM-12.html https://medkoo.com/products/11038 https://www.caymanchem.com/product/19480/cwhm12
NOTT199SS	School of Chemistry at the University of Nottingham	n/a
GM6001 (MMP inhibitor)	Sigma	Cat# CC1010
DharmaFECT 1 transfection reagent	Dharmacon	Cat# T-2001-01
10% formalin	VWR	Cat# 11699404
Mayers haematoxylin	Sigma	Cat# S1275
Eosin	VWR	Cat# 101411-524
Hydrogen peroxide	VWR	Cat# 23619.264
SIGMAFAST(TM) 3,3'-Diaminobenzidine tablets	Sigma	Cat# D4418
AEBSF (serine protease inhibitor	Sigma	Cat# SBR00015
Western Restore Stripping Buffer	Thermo-Fisher	Cat# 21059
Ferric chloride (Iron(III) chloride)	Sigma	Cat# 157740
Iodine	Sigma	Cat# 326143
Potassium iodide	Sigma	Cat# 03124
Picric acid (in aqueous solution)	VWR	Cat# 84512.260
Acid fuschin	Sigma	Cat# **F8129**

Direct red 80	Sigma	Cat# 365548
Sodium thiosulphate	Scientific Laboratory Supplies	Cat# 72049
Haematoxylin	Sigma	Cat# H3136
Experimental Models: Cell Lines		
Human lung fibroblasts – primary cultures	Isolated and cultured in house (see methods for details)	n/a
Murine embryonic fibroblasts – wild-type	(Gu et al., 2002; Zywietz et al., 2001)	n/a
Murine embryonic fibroblasts – $Gnaq^{-/-}Gna11^{-/-}$	(Gu et al., 2002; Zywietz et al., 2001)	n/a
Murine embryonic fibroblasts – $Gna12^{-/-};Gna13^{-/-}$	(Gu et al., 2002; Zywietz et al., 2001)	n/a
Experimental Models: Organisms/Strains		
Pdgfrb-$Cre^{+/-}$ mice	Generation described in (Foo et al., 2006)	n/a
$Gnaq^{fl/fl};Gna11^{-/-}$ mice	Generation described in (Offermanns et al., 1998; Wettschureck et al., 2001). Sperm stored in lab of origin.	n/a
Oligonucleotides		
Genotyping primers: Cre recombinase 5'- GCG GTC TGG CAG TAA AAA CTA TC – 3'; 5' - GTG AAA CAG CAT TGC TGT CAC TT – 3'	Eurofins (custom order)	n/a

Genotyping primers: internal positive control 5' - CTA GGC CAC AGA ATT GAA AGA TCT – 3' 5' - GTA GGT GGA AAT TCT AGC ATC ATC C – 3'	Eurofins (custom order)	n/a
Genotyping primers: Gna11 wild type 5' – AGC ATG CTG TAA GAC CGT AG - 3' 5' – GCC CCT TGT ACA GAT GGC AG – 3'	Eurofins (custom order)	n/a
Genotyping primers: Gna11 knockout 5' - CAG GGG TAG GTG ATG ATT GTG – 3' 5' – GAC TAG TGA GAC GTG CTA CTT CC - 3'	Eurofins (custom order)	n/a
Genotyping primers: Gnaq 5' – GCA TGC GTG TCC TTT ATG TGA G 3' 5' – AGC TTA GTC TGG TGA CAG AAG – 3'	Eurofins (custom order)	n/a
Human GNAQ siRNA (ON-TARGET-plus SMARTpool)	Dharmacon	Cat# L-008562-00-0005
Human GNA11 siRNA (ON-TARGET-plus SMARTpool)	Dharmacon	Cat# L-010860-00-0005
Non-targeting siRNA pool (ON-TARGET-plus SMARTpool)	Dharmacon	Cat# D-001810-10-05
Mouse Hprt primer forward: 5' – TGA AAG ACT TGC TCG AGA TGT CA - 3'	Eurofins (custom order)	n/a
Mouse Hprt primer reverse: 5' – CCA GCA GGT CAG CAA AGA ACT 3'	Eurofins (custom order)	n/a
Mouse Acta2 primer forward: 5' - GGG ATC CTG ACG CTG AAG TA – 3'	Eurofins (custom order)	n/a
Mouse Acta2 primer reverse: 5' – GAC AGC ACA GCC TGA ATA GC – 3'	Eurofins (custom order)	n/a
Mouse Eln primer forward: 5' GAT GGT GCA CAC CTT TGT TG 3'	Eurofins (custom order)	n/a

Mouse Eln primer reverse: 5' CAG TGT GAG GAG CCA TCT CA 3'	Eurofins (custom order)	n/a
Mouse Col1a1 primer forward: 5' AGC TTT GTG CAC CTC CGG CT 3'	Eurofins (custom order)	n/a
Mouse Col1a1 primer reverse: 5' ACA CAG CCG TGC CAT TGT GG 3'	Eurofins (custom order)	n/a
Mouse Col3a1 primer forward: 5' TTT GCA GCC TGG GCT CAT TT 3'	Eurofins (custom order)	n/a
Mouse Col3a1 primer: reverse: 5' AGG TAC CGA TTT GAA CAG ACT 3'	Eurofins (custom order)	n/a
Human GNAQ primer forward: 5' – GGACAGGAGAGGGTGGCAAG – 3'	Eurofins (custom order)	n/a
Human GNAQ primer reverse: 5' – TGGGATCTTGAGTGTGTCCA – 3'	Eurofins (custom order)	n/a
Human GNA11 primer forward: 5' – CCACTGCTTTGAGAACGTGA – 3'	Eurofins (custom order)	n/a
Human GNA11 primer reverse: 5' GCAGGTCCTTCTTGTTGAGG – 3'	Eurofins (custom order)	n/a
Human B2M primer forward: 5'-AATCCAAATGCGGCATCT-3'	Eurofins (custom order)	n/a
Human B2m primer reverse: 5'-GAGTATGCCTGCCGTGTG-3'	Eurofins (custom order)	n/a
Software and Algorithms		
Image J	NIH	https://imagej.nih.gov/ij/
NIH Elements v3.2	Nikon	https://www.microscope.healthcare.nikon.com/products/software/nis-elements/viewer

MicroManager 1.4	Vale lab, UCSF	https://micro-manager.org/
CaseViewer 2.3	3D Histech	https://www.3dhistech.com/
Prism	Graphpad	https://www.graphpad.com/scientific-software/prism/
Other		
Goat serum	Sigma	Cat# G9023
Avidin-Biotin complex	Vector	Cat# SP2001
DPX mountant	Sigma	Cat# 06522
Phosphate buffered saline	Sigma	Cat# P4417
Nikon 90i microscope	Nikon	n/a
Axioplan microscope	Zeiss	n/a
Dulbecco's modified eagles medium	Sigma	D5671
Foetal Calf Serum	Harlan UK Ltd	S-0001AE
L-glutamine	Sigma	G7513
Penicillin/ streptomycin	Sigma	P4458
Amphotericin B	Sigma	Cat# A2942
Collagen I-coated Bioflex® 6 well culture plates	Dunn Labortechnik	Cat# 3001-C
Flexcell® cell stretching system	Flexcell International Corporation	Cat# FX-5000T
BCA Assay kit	ThermoFisher	Cat# PN23227
Nucleospin RNA isolation kit	Machery-Nagel	Cat# 740955.250
Superscript IV Reverse Transcriptase	ThermoFisher	Cat# 18090050
KAPA SYBR FastTaq	Sigma	Cat# KK4618
MXPro3000 qPCR machine	Stratagene	
Heparin sodium 5000 units/ml	Wockhardt	Cat# FP1083

Polyvinylidene fluoride membrane	BioRad	Cat# 1620177
Hyperfilm for western blots	GE Healthcare	Cat# 28-9068-35
ECL reagent	GE Healthcare	Cat# RPN2134
Clarity ECL	BioRad	Cat# **1705061**

Supplemental Information titles and legends

Figure S1: Mice lacking mesenchymal $G_{\alpha q/11}$ do not have right ventricular hypertrophy

A) H&E staining of hearts from representative P14 *Gna11*$^{-/-}$ (top) and *Pdgfrb-Cre*$^{+/-}$;*Gnaq*$^{fl/fl}$;*Gna11*$^{-/-}$ (bottom) mice. Scale bar shows 1000µm

B) Right ventricular: left ventricular wall thickness ratios in P14 *Pdgfrb-Cre*$^{+/-}$;*Gnaq*$^{fl/fl}$;*Gna11*$^{-/-}$ (bottom) mice. Median ± interquartile range.

References

Alejandre-Alcázar, M.A., Michiels-Corsten, M., Vicencio, A.G., Reiss, I., Ryu, J., de Krijger, R.R., Haddad, G.G., Tibboel, D., Seeger, W., Eickelberg, O.*, et al.* (2008). TGF-beta signaling is dynamically regulated during the alveolarization of rodent and human lungs. Dev Dyn *237*, 259-269.

Barron, L., Gharib, S.A., and Duffield, J.S. (2016). Lung Pericytes and Resident Fibroblasts: Busy Multitaskers. Am J Pathol *186*, 2519-2531.

Bartram, U., and Speer, C.P. (2004). The role of transforming growth factor beta in lung development and disease. Chest *125*, 754-765.

Beauchemin, K.J., Wells, J.M., Kho, A.T., Philip, V.M., Kamir, D., Kohane, I.S., Graber, J.H., and Bult, C.J. (2016). Temporal dynamics of the developing lung transcriptome in three common inbred strains of laboratory mice reveals multiple stages of postnatal alveolar development. PeerJ *4*, e2318.

Belcastro, R., Lopez, L., Li, J., Masood, A., and Tanswell, A.K. (2015). Chronic lung injury in the neonatal rat: up-regulation of TGFβ1 and nitration of IGF-R1 by peroxynitrite as likely contributors to impaired alveologenesis. Free Radic Biol Med *80*, 1-11.

Bonniaud, P., Kolb, M., Galt, T., Robertson, J., Robbins, C., Stampfli, M., Lavery, C., Margetts, P.J., Roberts, A.B., and Gauldie, J. (2004). Smad3 null mice develop airspace enlargement and are resistant to TGF-beta-mediated pulmonary fibrosis. J Immunol *173*, 2099-2108.

Chen, H., Sun, J., Buckley, S., Chen, C., Warburton, D., Wang, X.F., and Shi, W. (2005). Abnormal mouse lung alveolarization caused by Smad3 deficiency is a developmental antecedent of centrilobular emphysema. Am J Physiol Lung Cell Mol Physiol *288*, L683-691.

Chen, H., Zhuang, F., Liu, Y.H., Xu, B., Del Moral, P., Deng, W., Chai, Y., Kolb, M., Gauldie, J., Warburton, D.*, et al.* (2008). TGF-beta receptor II in epithelia versus mesenchyme plays distinct roles in the developing lung. Eur Respir J *32*, 285-295.

Cheng, H.Y., Dong, A., Panchatcharam, M., Mueller, P., Yang, F., Li, Z., Mills, G., Chun, J., Morris, A.J., and Smyth, S.S. (2012). Lysophosphatidic acid signaling protects pulmonary vasculature from hypoxia-induced remodeling. Arterioscler Thromb Vasc Biol *32*, 24-32.

Dabovic, B., Chen, Y., Choi, J., Vassallo, M., Dietz, H.C., Ramirez, F., von Melchner, H., Davis, E.C., and Rifkin, D.B. (2009). Dual functions for LTBP in lung development: LTBP-4 independently modulates elastogenesis and TGF-beta activity. J Cell Physiol *219*, 14-22.

Deng, S., Zhang, H., Han, W., Guo, C., and Deng, C. (2019). Transforming Growth Factor-β-Neutralizing Antibodies Improve Alveolarization in the Oxygen-Exposed Newborn Mouse Lung. J Interferon Cytokine Res *39*, 106-116.

Donahoe, P.K., Longoni, M., and High, F.A. (2016). Polygenic Causes of Congenital Diaphragmatic Hernia Produce Common Lung Pathologies. Am J Pathol *186*, 2532-2543.

Foo, S.S., Turner, C.J., Adams, S., Compagni, A., Aubyn, D., Kogata, N., Lindblom, P., Shani, M., Zicha, D., and Adams, R.H. (2006). Ephrin-B2 controls cell motility and adhesion during blood-vessel-wall assembly. Cell *124*, 161-173.

Froese, A.R., Shimbori, C., Bellaye, P.S., Inman, M., Obex, S., Fatima, S., Jenkins, G., Gauldie, J., Ask, K., and Kolb, M. (2016). Stretch-induced Activation of Transforming Growth Factor-beta1 in Pulmonary Fibrosis. Am J Respir Crit Care Med *194*, 84-96.

Fujita, H., Hida, M., Kanemoto, K., Fukuda, K., Nagata, M., and Awazu, M. (2010). Cyclic stretch induces proliferation and TGF-beta1-mediated apoptosis via p38 and ERK in ureteric bud cells. Am J Physiol Renal Physiol *299*, F648-655.

Funke, M., Knudsen, L., Lagares, D., Ebener, S., Probst, C.K., Fontaine, B.A., Franklin, A., Kellner, M., Kuhnel, M., Matthieu, S.*, et al.* (2016). Lysophosphatidic Acid Signaling through the Lysophosphatidic Acid-1 Receptor Is Required for Alveolarization. Am J Respir Cell Mol Biol *55*, 105-116.

Furumatsu, T., Matsumoto, E., Kanazawa, T., Fujii, M., Lu, Z., Kajiki, R., and Ozaki, T. (2013). Tensile strain increases expression of CCN2 and COL2A1 by activating TGF-beta-Smad2/3 pathway in chondrocytic cells. J Biomech *46*, 1508-1515.

Gauldie, J., Galt, T., Bonniaud, P., Robbins, C., Kelly, M., and Warburton, D. (2003). Transfer of the active form of transforming growth factor-beta 1 gene to newborn rat lung induces changes consistent with bronchopulmonary dysplasia. Am J Pathol *163*, 2575-2584.

Gu, J.L., Muller, S., Mancino, V., Offermanns, S., and Simon, M.I. (2002). Interaction of G alpha(12) with G alpha(13) and G alpha(q) signaling pathways. Proc Natl Acad Sci U S A *99*, 9352-9357.

Harrell, C.R., Simovic Markovic, B., Fellabaum, C., Arsenijevic, A., Djonov, V., and Volarevic, V. (2018). Molecular mechanisms underlying therapeutic potential of pericytes. J Biomed Sci *25*, 21.

Henderson, N.C., Arnold, T.D., Katamura, Y., Giacomini, M.M., Rodriguez, J.D., McCarty, J.H., Pellicoro, A., Raschperger, E., Betsholtz, C., Ruminski, P.G.*, et al.* (2013). Targeting of

alphav integrin identifies a core molecular pathway that regulates fibrosis in several organs. Nat Med *19*, 1617-1624.

Hoyer, D.P., Gronke, S., Frank, K.F., Addicks, K., Wettschureck, N., Offermanns, S., Erdmann, E., and Reuter, H. (2010). Diabetes-related defects in sarcoplasmic Ca2+ release are prevented by inactivation of G(alpha)11 and G(alpha)q in murine cardiomyocytes. Mol Cell Biochem *341*, 235-244.

Jenkins, G. (2008). The role of proteases in transforming growth factor-beta activation. Int J Biochem Cell Biol *40*, 1068-1078.

John, A.E., Wilson, M.R., Habgood, A., Porte, J., Tatler, A.L., Stavrou, A., Miele, G., Jolly, L., Knox, A.J., Takata, M.*, et al.* (2016). Loss of epithelial Gq and G11 signaling inhibits TGFbeta production but promotes IL-33-mediated macrophage polarization and emphysema. Sci Signal *9*, ra104.

Kaartinen, V., Voncken, J.W., Shuler, C., Warburton, D., Bu, D., Heisterkamp, N., and Groffen, J. (1995). Abnormal lung development and cleft palate in mice lacking TGF-beta 3 indicates defects of epithelial-mesenchymal interaction. Nat Genet *11*, 415-421.

Kato, K., Dieguez-Hurtado, R., Park, D.Y., Hong, S.P., Kato-Azuma, S., Adams, S., Stehling, M., Trappmann, B., Wrana, J.L., Koh, G.Y.*, et al.* (2018). Pulmonary pericytes regulate lung morphogenesis. Nat Commun *9*, 2448.

Li, C., Li, M., Li, S., Xing, Y., Yang, C.Y., Li, A., Borok, Z., De Langhe, S., and Minoo, P. (2015). Progenitors of secondary crest myofibroblasts are developmentally committed in early lung mesoderm. Stem Cells *33*, 999-1012.

Maeda, T., Sakabe, T., Sunaga, A., Sakai, K., Rivera, A.L., Keene, D.R., Sasaki, T., Stavnezer, E., Iannotti, J., Schweitzer, R.*, et al.* (2011). Conversion of mechanical force into TGF-beta-mediated biochemical signals. Curr Biol *21*, 933-941.

Mecham, R.P. (2018). Elastin in lung development and disease pathogenesis. Matrix Biol *73*, 6-20.

Mizikova, I., and Morty, R.E. (2015). The Extracellular Matrix in Bronchopulmonary Dysplasia: Target and Source. Front Med (Lausanne) *2*, 91.

Nakanishi, H., Sugiura, T., Streisand, J.B., Lonning, S.M., and Roberts, J.D., Jr. (2007). TGF-beta-neutralizing antibodies improve pulmonary alveologenesis and vasculogenesis in the injured newborn lung. Am J Physiol Lung Cell Mol Physiol *293*, L151-161.

Offermanns, S., Zhao, L.P., Gohla, A., Sarosi, I., Simon, M.I., and Wilkie, T.M. (1998). Embryonic cardiomyocyte hypoplasia and craniofacial defects in G alpha q/G alpha 11-mutant mice. EMBO J *17*, 4304-4312.

Pakshir, P., Noskovicova, N., Lodyga, M., Son, D.O., Schuster, R., Goodwin, A., Karvonen, H., and Hinz, B. (2020). The myofibroblast at a glance. J Cell Sci *133*.

Patel, J.A., Shen, L., Hall, S.M., Benyahia, C., Norel, X., McAnulty, R.J., Moledina, S., Silverstein, A.M., Whittle, B.J., and Clapp, L.H. (2018). Prostanoid EP_2 Receptors Are Up-Regulated in Human Pulmonary Arterial Hypertension: A Key Anti-Proliferative Target for Treprostinil in Smooth Muscle Cells. Int J Mol Sci *19*.

Pelton, R.W., Dickinson, M.E., Moses, H.L., and Hogan, B.L. (1990). In situ hybridization analysis of TGF beta 3 RNA expression during mouse development: comparative studies with TGF beta 1 and beta 2. Development *110*, 609-620.

Pelton, R.W., Saxena, B., Jones, M., Moses, H.L., and Gold, L.I. (1991). Immunohistochemical localization of TGF beta 1, TGF beta 2, and TGF beta 3 in the mouse embryo: expression patterns suggest multiple roles during embryonic development. J Cell Biol *115*, 1091-1105.

Pieretti, A.C., Ahmed, A.M., Roberts, J.D., Jr., and Kelleher, C.M. (2014). A novel in vitro model to study alveologenesis . Am J Respir Cell Mol Biol *50*, 459-469.

Pozarska, A., Rodriguez-Castillo, J.A., Surate Solaligue, D.E., Ntokou, A., Rath, P., Mizikova, I., Madurga, A., Mayer, K., Vadasz, I., Herold, S.*, et al.* (2017). Stereological monitoring of mouse lung alveolarization from the early postnatal period to adulthood. Am J Physiol Lung Cell Mol Physiol *312*, L882-l895.

Ricard, N., Tu, L., Le Hiress, M., Huertas, A., Phan, C., Thuillet, R., Sattler, C., Fadel, E., Seferian, A., Montani, D.*, et al.* (2014). Increased pericyte coverage mediated by endothelial-derived fibroblast growth factor-2 and interleukin-6 is a source of smooth muscle-like cells in pulmonary hypertension. Circulation *129*, 1586-1597.

Russo, T.A., Stoll, D., Nader, H.B., and Dreyfuss, J.L. (2018). Mechanical stretch implications for vascular endothelial cells: Altered extracellular matrix synthesis and remodeling in pathological conditions. Life Sci *213*, 214-225.

Sanford, L.P., Ormsby, I., Gittenberger-de Groot, A.C., Sariola, H., Friedman, R., Boivin, G.P., Cardell, E.L., and Doetschman, T. (1997). TGFbeta2 knockout mice have multiple developmental defects that are non-overlapping with other TGFbeta knockout phenotypes. Development *124*, 2659-2670.

Sassmann, A., Gier, B., Grone, H.J., Drews, G., Offermanns, S., and Wettschureck, N. (2010). The Gq/G11-mediated signaling pathway is critical for autocrine potentiation of insulin secretion in mice. J Clin Invest *120*, 2184-2193.

Schmid, P., Cox, D., Bilbe, G., Maier, R., and McMaster, G.K. (1991). Differential expression of TGF beta 1, beta 2 and beta 3 genes during mouse embryogenesis. Development *111*, 117-130.

Shull, M.M., Ormsby, I., Kier, A.B., Pawlowski, S., Diebold, R.J., Yin, M., Allen, R., Sidman, C., Proetzel, G., Calvin, D.*, et al.* (1992). Targeted disruption of the mouse transforming growth factor-beta 1 gene results in multifocal inflammatory disease. Nature *359*, 693-699.

Sterner-Kock, A., Thorey, I.S., Koli, K., Wempe, F., Otte, J., Bangsow, T., Kuhlmeier, K., Kirchner, T., Jin, S., Keski-Oja, J.*, et al.* (2002). Disruption of the gene encoding the latent transforming growth factor-beta binding protein 4 (LTBP-4) causes abnormal lung development, cardiomyopathy, and colorectal cancer. Genes Dev *16*, 2264-2273.

Vicencio, A.G., Lee, C.G., Cho, S.J., Eickelberg, O., Chuu, Y., Haddad, G.G., and Elias, J.A. (2004). Conditional overexpression of bioactive transforming growth factor-beta1 in neonatal mouse lung: a new model for bronchopulmonary dysplasia? Am J Respir Cell Mol Biol *31*, 650-656.

Wang, B.W., Wu, G.J., Cheng, W.P., and Shyu, K.G. (2013). Mechanical stretch via transforming growth factor-beta1 activates microRNA-208a to regulate hypertrophy in cultured rat cardiac myocytes. J Formos Med Assoc *112*, 635-643.

Wettschureck, N., Lee, E., Libutti, S.K., Offermanns, S., Robey, P.G., and Spiegel, A.M. (2007). Parathyroid-specific double knockout of Gq and G11 alpha-subunits leads to a phenotype resembling germline knockout of the extracellular Ca2+ -sensing receptor. Mol Endocrinol *21*, 274-280.

Wettschureck, N., Moers, A., Hamalainen, T., Lemberger, T., Schutz, G., and Offermanns, S. (2004). Heterotrimeric G proteins of the Gq/11 family are crucial for the induction of maternal behavior in mice. Mol Cell Biol *24*, 8048-8054.

Wettschureck, N., Moers, A., Wallenwein, B., Parlow, A.F., Maser-Gluth, C., and Offermanns, S. (2005). Loss of Gq/11 family G proteins in the nervous system causes pituitary somatotroph hypoplasia and dwarfism in mice. Mol Cell Biol *25*, 1942-1948.

Wettschureck, N., Rutten, H., Zywietz, A., Gehring, D., Wilkie, T.M., Chen, J., Chien, K.R., and Offermanns, S. (2001). Absence of pressure overload induced myocardial hypertrophy after conditional inactivation of Galphaq/Galpha11 in cardiomyocytes. Nat Med *7*, 1236-1240.

Wettschureck, N., van der Stelt, M., Tsubokawa, H., Krestel, H., Moers, A., Petrosino, S., Schutz, G., Di Marzo, V., and Offermanns, S. (2006). Forebrain-specific inactivation of Gq/G11 family G proteins results in age-dependent epilepsy and impaired endocannabinoid formation. Mol Cell Biol *26*, 5888-5894.

www.ipfcellatlas.com (2020). IPF Cell Atlas Researchers. www.ipfcellatlas.com. Kaminski/Rosas dataset, N. N, ed.

www.lungmap.net. LungMAP consortium. www.lungmap.net, pp. The LungMAP consortium and the LungMAP Data Coordinating Center (1U01HL122638) are funded by the National Heart, Lung, and Blood Institute (NHLBI).

Xu, M.Y., Porte, J., Knox, A.J., Weinreb, P.H., Maher, T.M., Violette, S.M., McAnulty, R.J., Sheppard, D., and Jenkins, G. (2009). Lysophosphatidic acid induces alphavbeta6 integrin-mediated TGF-beta activation via the LPA2 receptor and the small G protein G alpha(q). Am J Pathol *174*, 1264-1279.

Zywietz, A., Gohla, A., Schmelz, M., Schultz, G., and Offermanns, S. (2001). Pleiotropic effects of Pasteurella multocida toxin are mediated by Gq-dependent and -independent mechanisms. involvement of Gq but not G11. J Biol Chem *276*, 3840-3845.

Fig 1

A)

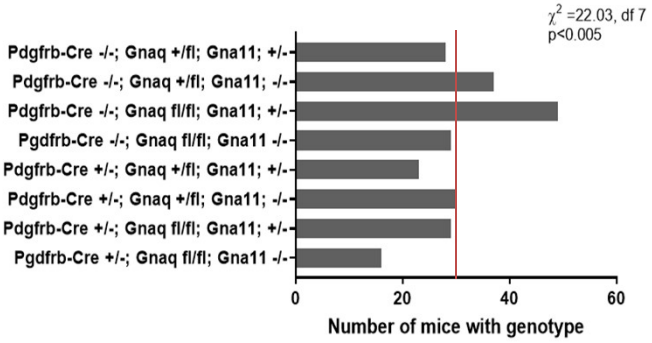

B)

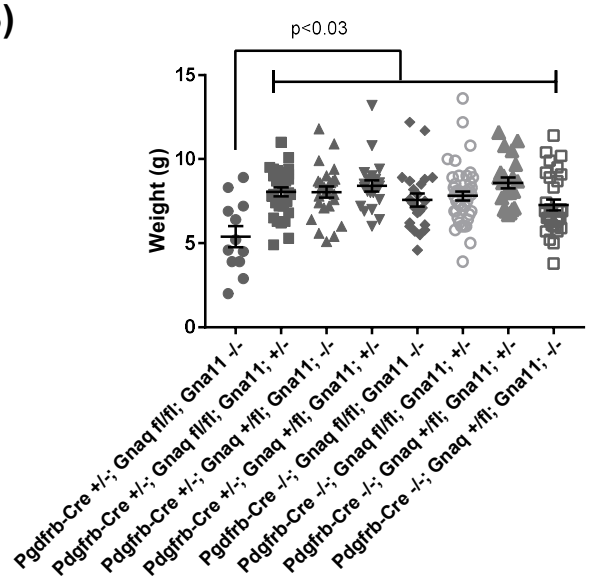

C)

Pdgfrb-Cre$^{+/-}$; Gnaq$^{fl/fl}$; Gna11$^{-/-}$

Pdgfrb-Cre$^{-/-}$; Gnaq$^{fl/fl}$; Gna11$^{-/-}$

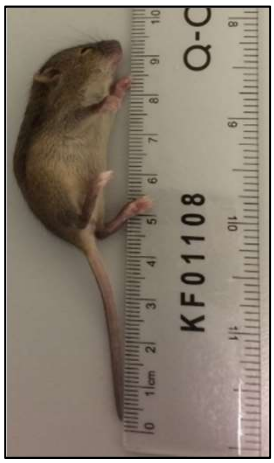

D)

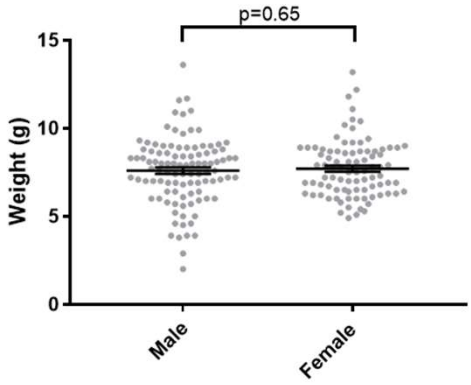

Fig 2

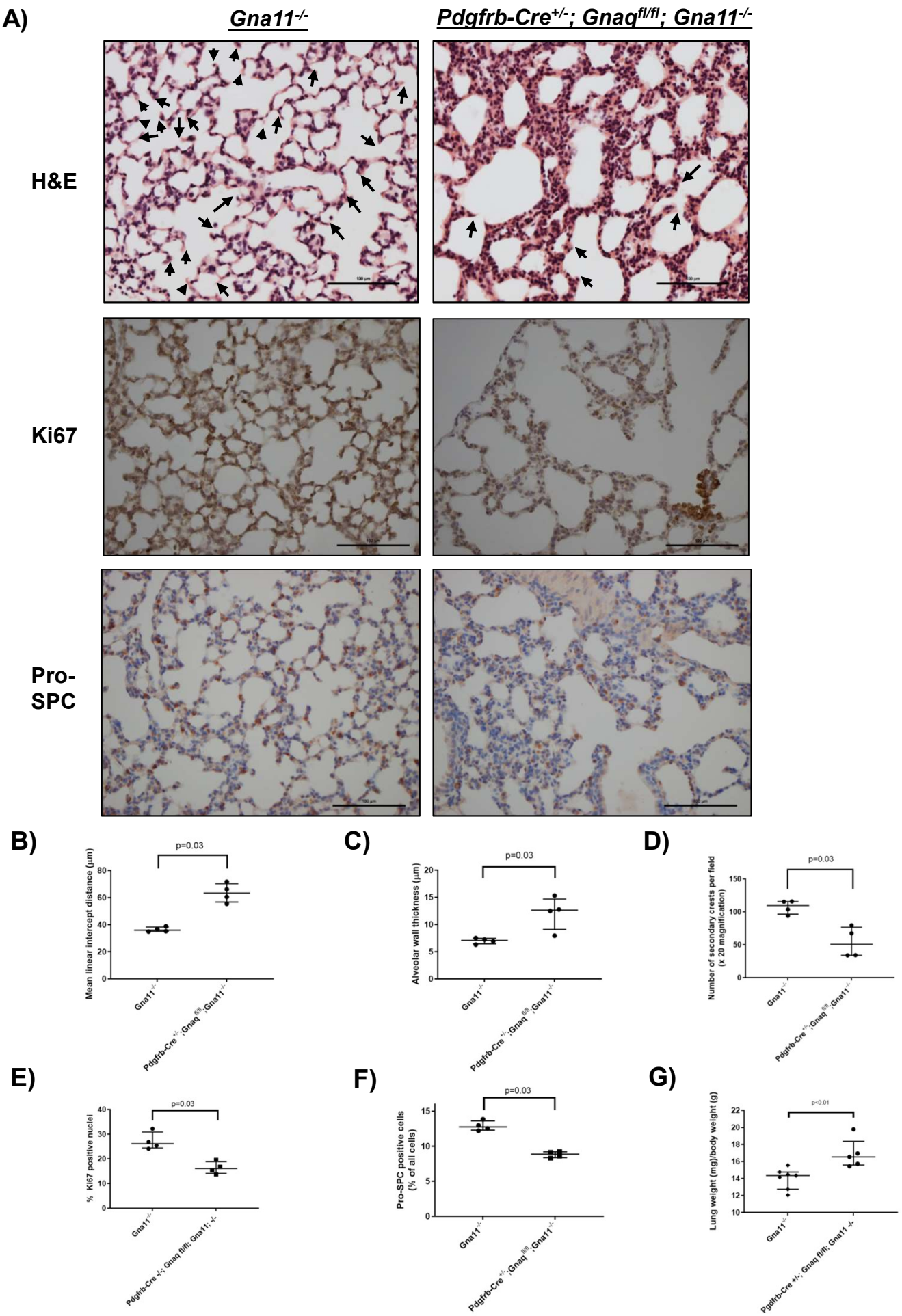

Fig 3

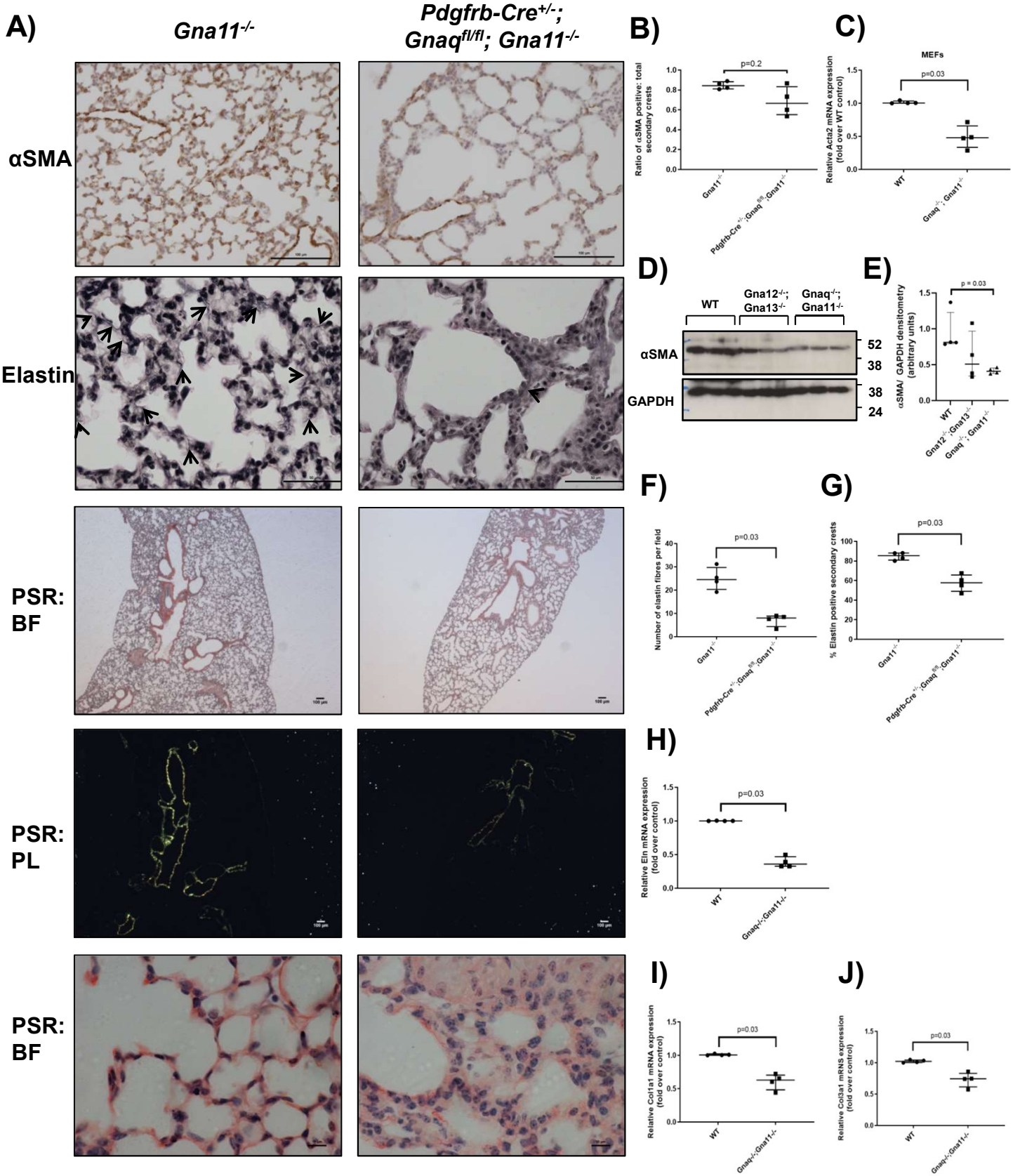

Fig 4

A)

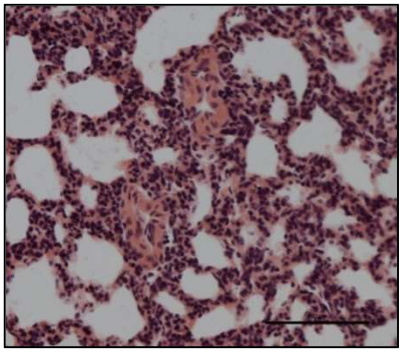

B)

Elastin

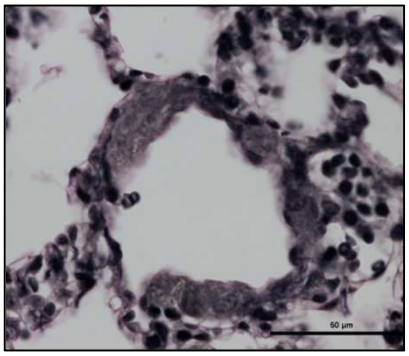

C)

PSR: BF

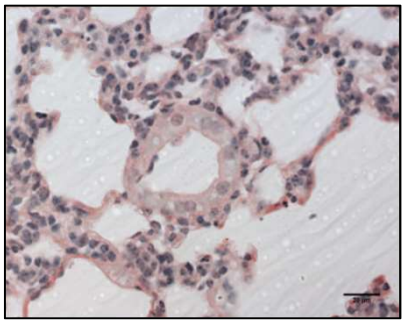

PSR: PL

D)

CD31

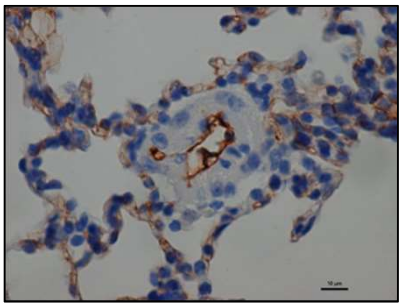

E)

αSMA

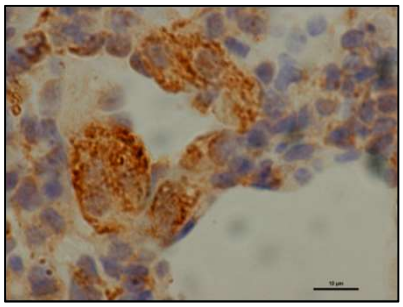

F)

Ki67

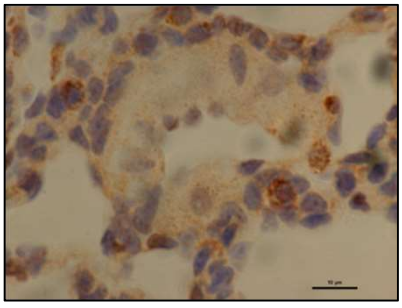

G)

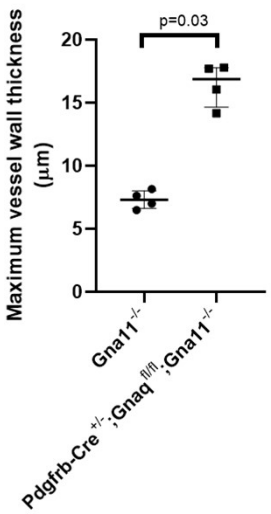

H)

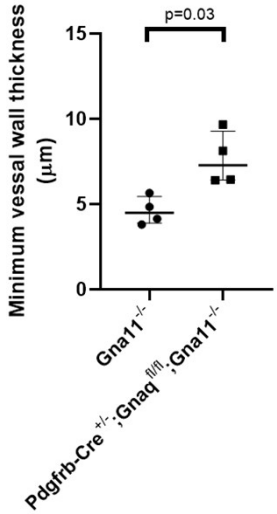

Fig 5

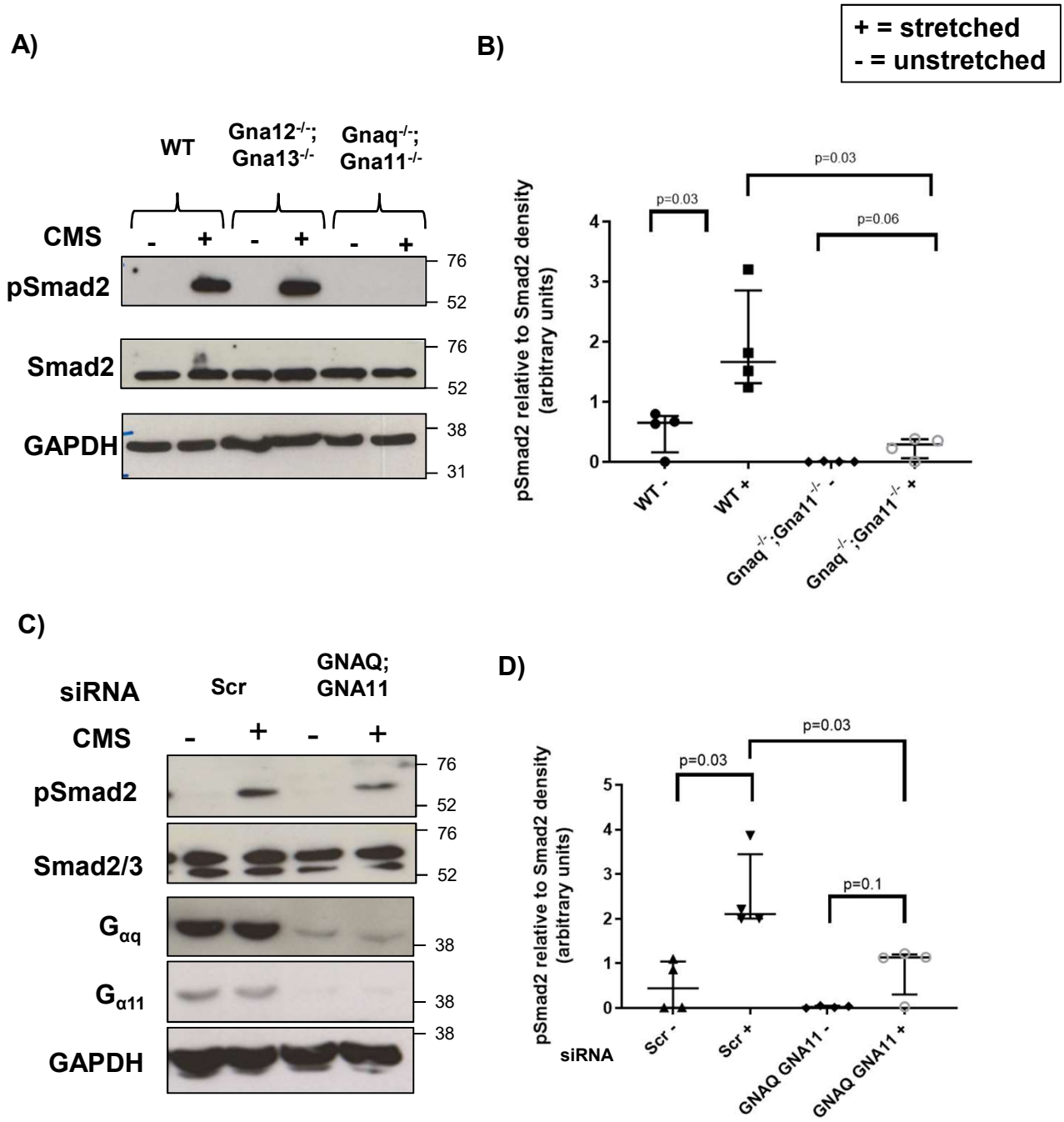

Fig 6

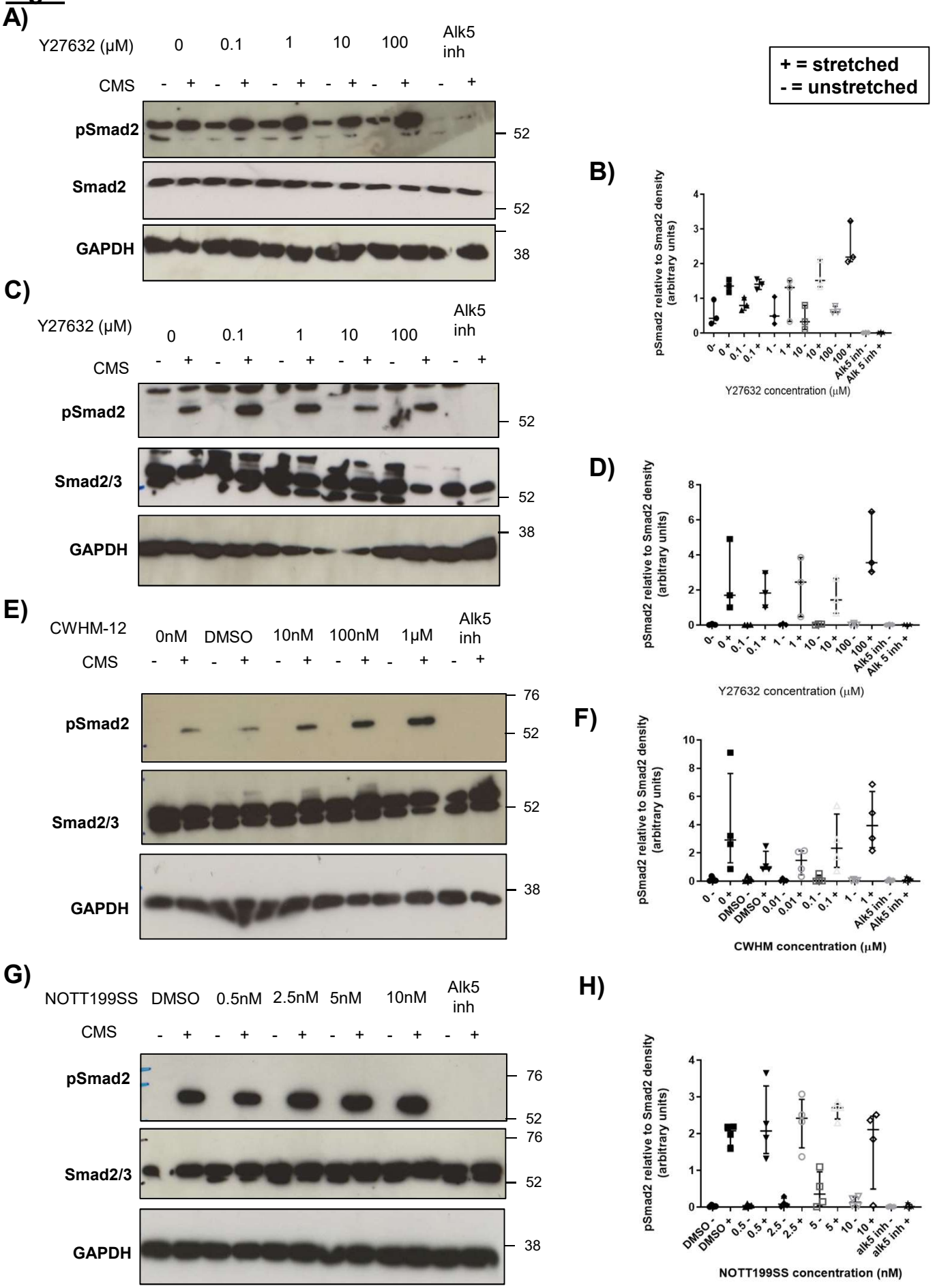

Fig 7